

# Optimizing Prussian Blue Analogues for Potassium-Ion Batteries: Advanced Strategies

Zihao Hu,<sup>[a]</sup> Bo Zhang,<sup>[a]</sup> Hehe Zhang,<sup>\*[a]</sup> and Yanjiao Ma<sup>\*[a]</sup>

Potassium-ion batteries (PIBs), with the merits of abundant resources and low cost, have rapidly garnered attention as a potential candidate for large-scale energy storage. Among the various contenders, Prussian blue analogues (PBAs) are considered one of the most suitable cathode materials owing to their relatively easy and economical synthesis as well as the three-dimensional open framework which facilitates fast potassium ions intercalation without causing drastic volume expansion. Despite these advantages, integrating PBA as a cathode material for PIBs presents substantial challenges, which hinder

their further practical applications. Herein, a fundamental review on the development and advance of PBAs in PIBs is presented with the elucidation of their synthesis methods, structural characteristics, and optimization strategies. Particularly, key areas of focus include regulating crystal structures, doping transition metals, engineering interfaces, and employing innovative techniques such as high-entropy approaches are highlighted. Finally, critical perspectives for future development of PBAs toward practical potassium-based energy storage devices are proposed.

## 1. Introduction

The development of large-scale energy storage systems based on lithium-ion batteries (LIBs) has become inevitable due to their widespread use in various applications, from portable electronics to electric vehicles.<sup>[1]</sup> However, the limited and uneven distribution of lithium resources has driven the search for low-cost and abundant alternatives.<sup>[2–6]</sup> Among these, potassium metal has garnered significant interest. Potassium, a widely available alkali metal, shares similar physicochemical properties with lithium, making it a noteworthy alternative. Potassium's advantages over other substitutes are significant. Its standard oxidation-reduction potential of  $-2.94$  V vs. SHE is close to that of  $\text{Li}^+/\text{Li}$  ( $-3.04$  V vs. SHE).<sup>[7]</sup> Additionally,  $\text{K}^+$  have higher ionic conductivity than  $\text{Li}^+$  due to their lower solvation energy and reduced Lewis acidity, resulting in a smaller Stoke's radius.<sup>[8]</sup> Moreover, in contrast to lithium, potassium does not form aluminum-potassium alloys at low voltages, reducing potential losses.<sup>[9–12]</sup> This characteristic allows for the use of lightweight and cost-effective aluminum foil instead of copper foil in current collectors, thereby decreasing production costs of large-scale manufacturing. Potassium-ion batteries (PIBs) hold significant promise for low-cost, high-power density energy storage and conversion.<sup>[13]</sup> However, several challenges impede their widespread commercialization. The mass-to-charge ratio of  $\text{K}^+$  (39.1) is substantially higher than that of  $\text{Li}^+$  (6.94), which leads to instability in electrode materials and sluggish reaction kinetics during cycling, amplifying volume changes.<sup>[14]</sup> Despite these challenges, notable progress has been made in developing the negative electrode for PIBs, with graphite emerging as a

viable material.<sup>[15]</sup> This suggests that established lithium-ion systems can be adapted for potassium-ion use, leveraging advancements in high-capacity negative electrode materials from lithium-ion research. However, the positive electrode materials play a more pivotal role in influencing the overall capacity and performance of potassium-ion batteries.<sup>[16]</sup>

Recent advancements in positive electrode materials for PIBs have classified them into four main categories: layered metal oxides, polyanionic compounds, organic compounds, and Prussian blue (PB) and its analogues.<sup>[17]</sup> Layered metal oxides initially garnered attention due to their high tap density and theoretical specific capacity. However, they encounter challenges such as low  $\text{K}^+$  content, which diminishes overall battery performance, as well as suboptimal working potentials and irreversible phase transitions during cycling that affect stability. Polyanionic compounds, incorporating variants of vanadium and iron, exhibit reasonable electrochemical activity in PIBs but suffer from reduced specific capacity due to large anionic groups, limiting further development. Organic compounds, despite being cost-effective and environmentally benign, lack potassium, resulting in lower working voltages and poorer cycling performance. Moreover, their solubility in electrolytes poses significant challenges, compromising overall electrochemical efficiency. Conversely, Prussian Blue analogues (PBAs) present a compelling alternative with several distinct advantages: (i) Various synthesis routes for PBAs, such as co-precipitation, hydrothermal synthesis, and ball milling, offer flexibility in production.<sup>[18]</sup> Co-precipitation stands out for its simplicity, scalability, and cost-effectiveness, whereas hydrothermal synthesis, while yielding highly crystalline products, involves toxic by-products unsuitable for large-scale applications. (ii) PBA synthesis predominantly utilizes aqueous precipitation, minimizing costs associated with high-temperature processes and raw materials compared to conventional metal oxides and polyanionic compounds. This method leverages abundant and economical metal salts and hexacyanoferrate

[a] Z. Hu, B. Zhang, H. Zhang, Y. Ma

School of Energy and Mechanical Engineering, Nanjing Normal University,  
Nanjing 210023, China  
E-mail: hhzhang@njnu.edu.cn  
yanjiao.ma@njnu.edu.cn

complexes. (iii) The open framework structure of PBAs features numerous vacant sites conducive to alkali metal deintercalation.<sup>[19]</sup> This architecture supports efficient ionic transport, ensuring robust K<sup>+</sup> transmission and diffusion throughout the material, thereby enhancing long-term cycling stability.

Despite these advantages, integrating PBA as a positive electrode material for PIBs presents substantial challenges. The wet chemical synthesis process often introduces crystal water and structural defects due to rapid nucleation and growth kinetics, necessitating meticulous investigation to optimize PIB performance.<sup>[20]</sup> Furthermore, the elevated operational voltages of PIBs can trigger irreversible electrolyte decomposition, exacerbating secondary reactions and safety concerns. Specific challenges include: (1) Rapid precipitation methods in PBA synthesis may introduce defects and vacancies in the crystal lattice, notably Fe(CN)<sub>6</sub><sup>4-</sup> vacancies that enhance ionic conductivity but potentially compromise structural stability.<sup>[21]</sup> Water molecules occupying these vacancies can impede K<sup>+</sup> ion migration, impacting electrochemical kinetics. (2) PBA materials exhibit multiple phase transitions during K<sup>+</sup> ion insertion and extraction, involving cubic, monoclinic, and orthorhombic phases.<sup>[22]</sup> These transitions induce volume changes, posing significant stability challenges crucial for sustained cycling performance. (3) Manganese-based PBAs demonstrate promising high specific capacities but face challenges in long-term cycling due to Jahn-Teller distortions during K<sup>+</sup> insertion.<sup>[23]</sup>

These distortions induce structural deformations and phase transitions among cubic, monoclinic, and orthorhombic crystal systems, impacting overall battery performance.

In conclusion, this paper aims to comprehensively explore synthesis methods, structural characteristics, and optimization strategies for PBAs as positive electrode materials in PIBs. Key areas of focus include regulating crystal structures, doping transition metals, engineering interfaces, and employing innovative techniques such as high-entropy approaches. By tackling challenges such as defects, managing water content and understanding phase transition dynamics, this review integrates recent advancements in crystallography, synthesis methodologies, and modification strategies for both PB and PBAs. These efforts not only aim to advance scientific understanding but also facilitate practical applications in PIB technology, thereby driving progress in both research and commercialization endeavors within the field.

## 2. Chemical Composition and Structure for PBAs

### 2.1. The History of PBAs in PIBs

The historical trajectory of PB spans centuries and encompasses a diverse array of applications across various fields. Originally



Zihao Hu is currently a Master's student at the School of Energy and Mechanical Engineering, Nanjing Normal University. His research primarily focuses on potassium-based Prussian blue materials and their applications in potassium metal batteries.



Bo Zhang is currently a Master's student at the School of Energy and Mechanical Engineering, Nanjing Normal University. His research primarily focuses on the design and synthesis of anode materials for sodium- and potassium-ion batteries.



Hehe Zhang received his Ph.D. degree in materials science and engineering from Xiamen University in 2023. He then joined the School of Energy and Mechanical Engineering at Nanjing Normal University. His research focuses on new electrode material preparation technology and unravelling the intricate failure mechanism of sodium/potassium-ion batteries.



Yanjiao Ma is currently a Professor at Nanjing Normal University. Prior to this, she was a postdoctoral researcher at the Institute of Nanotechnology (INT), Karlsruhe Institute of Technology (KIT), where she specialized in developing advanced functional materials, including high-entropy materials for various battery technologies, and mesostructured metal oxide thin films. In 2019, she completed her Ph.D. in Physical Chemistry at the Helmholtz Institute Ulm/KIT, under the mentorship of Prof. Passerini and Dr. Bresser, focusing on nanostructured materials for alkali-ion batteries.

discovered as the first synthetic pigment in the 18th century, PB has evolved into a versatile material with wide-ranging uses from biosensing and cancer treatment to energy storage and smart window technologies. In recent years, PB has also been adapted as a nanomaterial for advanced cancer therapies, leveraging its photothermal and photodynamic properties to enhance treatment precision and effectiveness. Additionally, PB plays pivotal roles in biocatalysis, biosensors, and optical electrochromic devices, highlighting its versatility and relevance in modern technologies.

PB's entry into energy storage technologies, particularly in rechargeable batteries, represents a significant milestone in its application history.<sup>[33]</sup> Recognized for its exceptional electrochemical properties, PB has been extensively investigated for its potential to enhance energy density and battery cycle life.<sup>[34]</sup> This exploration led to the development of PBAs, which initially garnered attention as electrode materials for LIBs around 1999.<sup>[35]</sup> However, PBAs have encountered challenges in achieving competitive lithium storage capacities compared to existing materials, thus limiting their integration into commercial LIBs and their exploration in sodium-ion batteries (SIBs) to advanced stages of development.<sup>[36]</sup> A pivotal moment arrived in 2004 with the assembly of potassium ion half-cells using PB as the cathode material, potassium metal as the anode, and specific electrolytes (Figure 1a).<sup>[24]</sup> This pioneering use of PBAs in PIBs marked their debut in the emerging energy storage sector. Despite initial setbacks due to potassium's large atomic radius,

which posed challenges for efficient ion insertion and diffusion, subsequent years witnessed persistent efforts to overcome these obstacles (Figure 1).<sup>[17]</sup>

Recent breakthroughs in optimizing PBAs' structural and compositional deficiencies have rekindled interest in their application for PIBs.<sup>[35]</sup> These optimization strategies have substantially enhanced potassium storage stability and performance, addressing longstanding barriers and bolstering the feasibility of PBAs for practical battery applications.<sup>[37]</sup> As researchers continue to refine PBAs through precise crystallographic control, transition metal doping, and innovative interface engineering, the future holds promising prospects for integrating PBAs into advanced PIB technologies.<sup>[20]</sup>

## 2.2. Fundamental Structure of PBAs

Potassium-based Prussian Blue and its analogues are hexacyanoferrate compounds, typically expressed by the chemical formula  $K_xM[M'(CN)_6]_y \square_{1-y} \cdot mH_2O$  ( $0 \leq x \leq 2$ ,  $y < 1$ ).<sup>[38,39]</sup> In this formula, K denotes potassium, which can be replaced by lithium or sodium in other systems; M represents transition metals such as Fe, Co, Ni, Mn, and Cu; M' usually refers to Fe, coordinating with the C atom in the CN ligands;  $\square$  signifies vacancies in the  $M'(CN)_6$ ; and  $H_2O$  includes both interstitial and coordinated water molecules (see Figure 2a).<sup>[40]</sup> Due to variations in M and M' types and their ratios, these compounds can adopt diverse

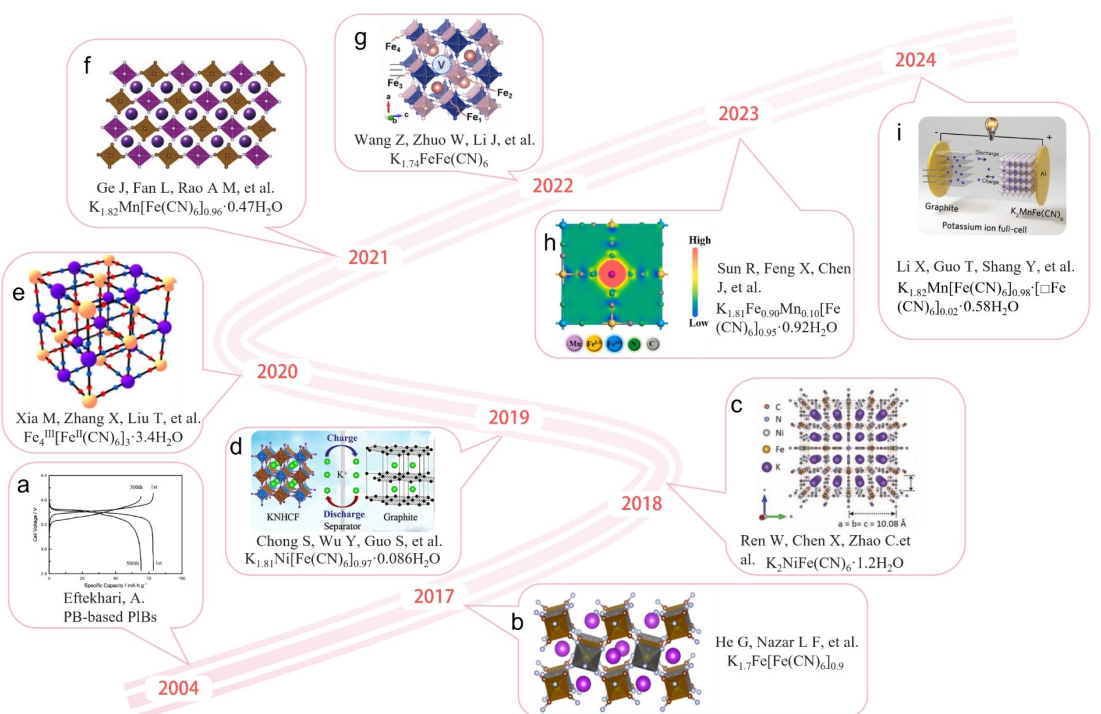


**Figure 1.** The evolution of PBAs in PIBs: a) PBAs were first employed as a cathode material in PIBs by Eftekhari.<sup>[24]</sup> b) Different grain sizes of PW were synthesized via solution chemistry methods.<sup>[25]</sup> c) Ultra-fast aqueous potassium-ion batteries were developed based on potassium-rich mesoporous nickel ferrocyanide.<sup>[26]</sup> d) Ni-PBA demonstrated an ultra-stable framework structure.<sup>[27]</sup> e) Commercial PB exhibited commendable performance in aqueous PIBs.<sup>[28]</sup> f) Mn-PBA partially substituted with Fe showed high electrochemical performance.<sup>[29]</sup> g) Low-defect Fe-PBA was synthesized with the aid of EDTA-2 K.<sup>[30]</sup> h) Mn substitution in Fe-PBA can effectively enhance conductivity and  $K^+$  transport kinetics.<sup>[31]</sup> i) Sodium citrate and high-temperature treatment collaboratively assisted in repairing vacancies in Mn-PBA.<sup>[32]</sup> Reproduced with permission.<sup>[24–32]</sup> Copyright 2004–2024, Elsevier, American Chemical Society, American Association for the Advancement of Science, Royal Society of Chemistry, Wiley-VCH.

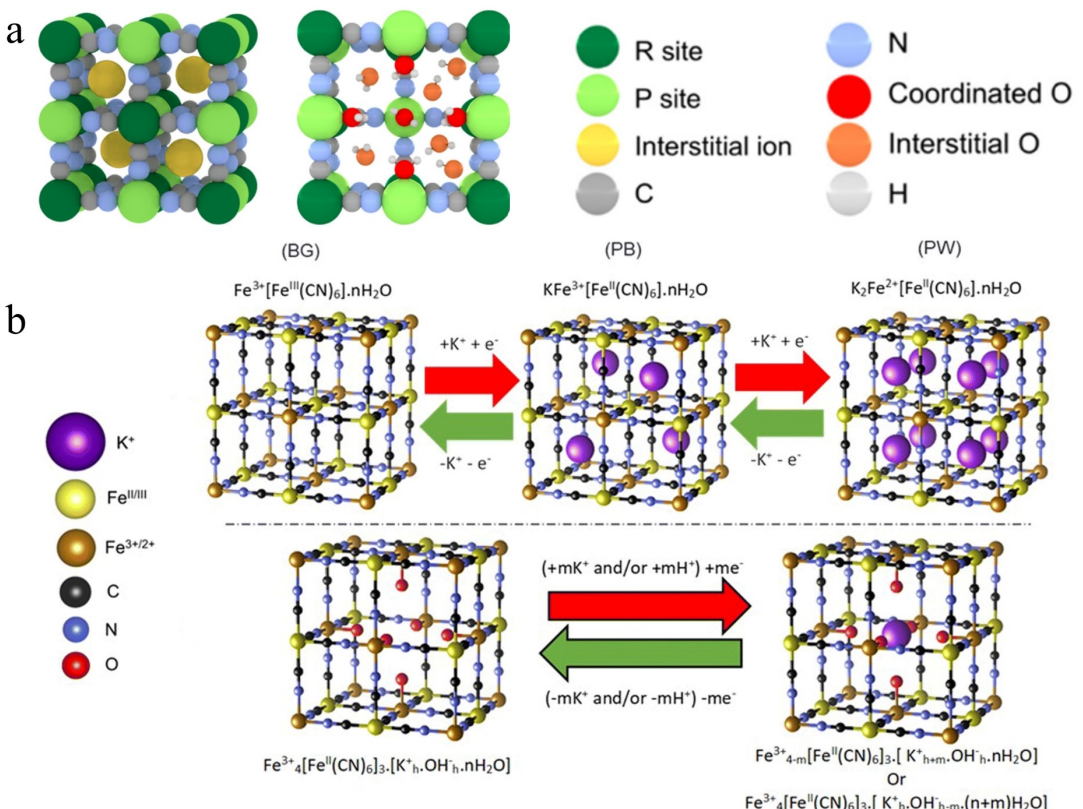


**Figure 2.** a) Schematic representation of cubic PBAs.<sup>[40]</sup> b) Ideal defect free Prussian blue and defective structure based on a  $[\text{Fe}^{\text{II}}(\text{CN})_6]^{4-}$  absence.<sup>[41]</sup> Reproduced with permission.<sup>[40,41]</sup> Copyright 2019–2023, American Chemical Society, Royal Society of Chemistry.

crystal phases, including monoclinic, cubic, and orthorhombic systems.

PBAs can also be classified based on their potassium content (see Figure 2b),<sup>[41]</sup> including Prussian White (PW:  $K_2Fe^{II}Fe^{II}(CN)_6 \cdot mH_2O$ ), which contains the highest potassium content;<sup>[25]</sup> PB ( $KFe^{III}Fe^{II}(CN)_6 \cdot mH_2O$ ), which has partial potassium content; and Berlin Green (BG:  $Fe^{III}Fe^{III}(CN)_6 \cdot mH_2O$ ), which has negligible or no potassium content.<sup>[42]</sup> The parameters x, y, and m in the general formula are significantly influenced by the synthesis conditions, transition metal ion properties, and the potassium content.<sup>[43]</sup> Generally, a high crystallization water content (high m value) corresponds to a lower potassium content (low x value) or more M'(CN)<sub>6</sub> vacancies (high y value).

PBAs typically exhibit a face-centered cubic perovskite structure, reminiscent of metal-organic framework (MOF) materials.<sup>[44]</sup> Within this crystalline framework, M and M' ions alternate at the lattice vertices, each coordinated octahedrally by six adjacent CN ligands composed of C and N atoms. These interconnected octahedra construct a sturdy 3D lattice featuring open ion transport channels and capacious voids capable of hosting both K<sup>+</sup> ions and crystallization water molecules.<sup>[45]</sup> This structural arrangement inherently facilitates rapid ion diffusion kinetics,<sup>[22]</sup> thereby promoting efficient K<sup>+</sup> ion insertion and extraction processes. Moreover, the robust integrity of the lattice structure effectively withstands mechanical stresses

induced by repetitive  $K^+$  ion cycling, ensuring exceptional long-term stability.<sup>[11]</sup>

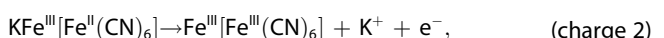
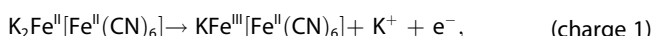
Interestingly, PIBs prefer PBA as electrode material compared to lithium and sodium.<sup>[35]</sup> The favorable accommodation of K ions within PBA cavities results in a more stable structure, offering PIBs higher redox voltages and improved cycling stability compared to LIBs and SIBs.<sup>[16]</sup> Despite the theoretical advantages of PBAs in potassium storage, practical synthesis often yields imperfect crystal structures due to rapid precipitation methods.<sup>[46]</sup> These methods introduce significant defects and vacancies, notably  $\text{Fe}(\text{CN})_6$  vacancies, which can destabilize the lattice and cause structural collapse during cycling.<sup>[47]</sup> These vacancies often trap water molecules during synthesis, forming coordinated water that obstructs  $\text{K}^+$  ion migration and slows reaction kinetics.<sup>[48]</sup> Moreover, the compromised structure can dissolve into the electrolyte, triggering further degradation and hindering redox reactions, thereby reducing potassium storage capacity.<sup>[49]</sup> Since the inception of PBA research for PIB applications, efforts have concentrated on optimizing the material to mitigate these detrimental effects. Addressing  $\text{Fe}(\text{CN})_6$  vacancies, which are primary structural defects, is crucial.<sup>[50]</sup> Their presence not only increases coordinated water content, impeding ion migration, but also distorts the framework, potentially leading to irreversible ion insertion and extraction.<sup>[20]</sup> Recent research focuses on minimizing these

defects during initial synthesis to enhance PBA stability and performance.<sup>[19]</sup>

In addition to vacancies, crystallization water within PBAs poses significant challenges. This water comprises adsorbed, interstitial, and coordinated forms, which can be partially removed by increasing synthesis temperatures.<sup>[51]</sup> However, higher temperatures required to eliminate interstitial water may compromise the structural integrity of PBAs.<sup>[19,52,53]</sup> The relationship between vacancies and crystallization water is intertwined; more vacancies lead to increased coordinated water, forming strong bonds with metal ions.<sup>[54]</sup> Current studies indicate that nearly all side reactions during K<sup>+</sup> insertion and extraction in PBAs are linked to crystallization water and vacancies.<sup>[20]</sup> Therefore, ongoing research aims to refine synthesis processes to minimize these issues, ultimately enhancing the electrochemical performance of PBAs in PIBs.

### 2.3. Potassium Storage Mechanism

The electrochemical behavior of PBAs hinges on their structural composition, notably the presence of transition metals (M and M') that participate in redox reactions.<sup>[55]</sup> PBAs encompass multiple redox types involving metals like Fe, Mn, and Co, which undergo electrochemical transformations, and single redox types involving metals like Ni, Cu, and Zn, which remain inert.<sup>[56]</sup> The energy density of PBAs correlates with their plateau potentials during charge and discharge cycles, with higher potentials indicating greater energy storage capacity.<sup>[57]</sup> Therefore, optimizing PBAs to maximize their potassium content (K<sup>+</sup>) is pivotal for augmenting their electrochemical performance in PIB applications. In a typical PBA structure with ideal stoichiometry ( $x=2, y=0$ ) and no crystallization water interaction (using K<sub>2</sub>Fe[Fe(CN)<sub>6</sub>] as a reference), the overall electrochemical equation governing K<sup>+</sup> insertion can be described as follows:



During the charging process, the initial departure of a K<sup>+</sup> ion from the lattice prompts the oxidation of Fe<sup>2+</sup> ions coordinated with nitrogen (N), marking the onset of the first potential plateau as voltage increases.<sup>[58]</sup> With further voltage elevation, a second K<sup>+</sup> ion exits the lattice, oxidizing Fe<sup>2+</sup> ions coordinated with carbon (C) and establishing the second potential plateau. Conversely, during discharge, K<sup>+</sup> ions reintegrate into the lattice, initiating reduction reactions involving Fe<sup>3+</sup> ions coordinated with both C and N. In PBAs containing electrochemically inert ions like Ni<sup>2+</sup>, only the M' ions participate in redox reactions during charge and discharge cycles.

Fe-PBA (KxFe[Fe(CN)<sub>6</sub>]) has garnered significant attention due to its low redox potential and superior cycling stability,

making them some of the earliest and most extensively studied materials within this category.<sup>[59]</sup> Mn-PBA (KxMn[Fe(CN)<sub>6</sub>]), on the other hand, exhibits two discharge plateaus during charge and discharge cycles. However, prolonged cycling often results in the dissolution of Mn into the electrolyte, leading to a gradual decline in reversible capacity.<sup>[60]</sup> Moreover, the presence of Mn may induce the Jahn-Teller effect, which compromises the lattice integrity. Despite these challenges, PBAs generally offer higher specific capacities for K<sup>+</sup> intercalation compared to traditional PIB oxide cathode materials. Enhancing the stability and electrochemical performance of PBAs involves strategic manipulation of the transition metal elements to meet specific battery application requirements.<sup>[61]</sup> A deep understanding of the complex mechanisms governing K<sup>+</sup> insertion and extraction in PBAs is pivotal for the development of high-performance PIB technologies.<sup>[62]</sup> PBAs can crystallize in various structural forms, such as monoclinic, cubic, and orthorhombic systems, with these variations being influenced by factors like defects, crystallization water content, K<sup>+</sup> concentration, and temperature.<sup>[49]</sup> The dynamic structural changes that occur during the charge and discharge cycles in PBAs are intricate and not yet fully elucidated, even in the more thoroughly examined SIB systems.<sup>[21]</sup> A significant challenge lies in the large ionic radius of K<sup>+</sup>, which induces substantial structural transformations during each insertion and extraction cycle.<sup>[63]</sup> To achieve a comprehensive understanding of how the PIB internal structure responds to these factors, researchers employ a suite of advanced *in-situ* and *ex-situ* techniques. These include X-ray diffraction (XRD), Raman spectroscopy, infrared spectroscopy, and X-ray absorption spectroscopy. Such methodologies are crucial for optimizing and developing high-performance electrode materials for the next generation of rechargeable batteries.<sup>[64]</sup>

### 3. Synthesis Methods of PBAs

The synthesis of PBAs is generally based on the chemical reactions between transition metal ions and [Fe(CN)<sub>6</sub>]<sup>3-</sup> or [Fe(CN)<sub>6</sub>]<sup>4-</sup>, which are extensive and cost-effective. The raw materials for K-PBAs commonly include K<sub>4</sub>Fe(CN)<sub>6</sub>, various transition metal salts (such as chlorides, sulfates, and nitrates of Fe, Mn, Co, Ni, Cu, Zn, etc.), and chelating agents like ethylene diamine tetraacetic acid (EDTA) and potassium citrate. Currently, there are primarily two synthetic methods for preparing PBAs, i.e., hydrothermal and co-precipitation methods, along with other techniques applied in different fields such as microwave-assisted and electrodeposition methods. Through selecting appropriate synthesis method, PBAs with different morphologies and structures can be obtained to tailor their electrochemical properties. Subsequent sections will delve into a detailed discussion of the two synthesis methods for preparing PBAs in PIBs research: hydrothermal and co-precipitation methods.

### 3.1. Hydrothermal Method

The hydrothermal synthesis of PBAs in current PIB research is relatively rare due to its low yield and the potential release of toxic hydrogen cyanide during the production process.<sup>[49]</sup> Despite this, the high quality of PBAs synthesized *via* hydrothermal methods has led to their use in laboratory environments for studying detailed potassium storage mechanisms. Li et al.<sup>[65]</sup> synthesized potassium Prussian white analogues (K-PW) with different crystallinity and size gradients by adjusting the acidity of the hydrothermal environment. The results showed that as the concentration of hydrochloric acid increased, the crystal size decreased, the particle morphology became irregular, and aggregation became more apparent. This was primarily because  $[\text{Fe}(\text{CN})_6]^{4-}$  slowly decomposed into  $\text{Fe}^{2+}$  in an acidic environment and then reacted with the undecomposed  $[\text{Fe}(\text{CN})_6]^{4-}$  to form Prussian white particles. As a result,  $\text{K}_{1.93}\text{Fe}[\text{Fe}(\text{CN})_6]_{0.97}1.82\text{H}_2\text{O}$  synthesized under a hydrochloric acid concentration of  $1 \text{ mol L}^{-1}$  exhibited a significant reversible capacity of  $142 \text{ mAh g}^{-1}$  at a current density of  $75 \text{ mA g}^{-1}$ , outperforming the currently reported K-PWs.

### 3.2. Precipitation Method

Compared to hydrothermal methods, precipitation methods are the most common and commercially promising approach for producing PBAs, as evidenced by a large number of studies. These methods include direct precipitation, co-precipitation, and acid-assisted co-precipitation. Currently, researchers widely choose the co-precipitation method for the synthesis of PBAs.<sup>[43]</sup> For example, Jung et al.<sup>[66]</sup> dissolved 2 mmol of potassium hexacyanoferrate in 100 ml of deionized water (Figure 3a). A separate solution was prepared by dissolving 2 mmol of manganese chloride and 4 mmol of potassium citrate in 100 ml of deionized water, which was then slowly added to the potassium hexacyanoferrate solution. The high concentration of

potassium citrate provided a potassium-rich environment that facilitated horizontal crystal growth, resulting in potassium-rich Prussian blue nanoplates. Compared to traditionally synthesized Prussian blue cubes, the obtained nanoplates exhibited significantly larger particle sizes. The thin plate-shaped KMnFe-PBA (PNP) minimized water-related side effects, demonstrating excellent specific capacity ( $152.5 \text{ mAh g}^{-1}$ ) and energy density ( $602.7 \text{ Wh kg}^{-1}$ ). Analogously, Liu et al.<sup>[67]</sup> proposed a simple and practical dual-salt-assisted co-precipitation method to synthesize PBA with high potassium content, low water content, and excellent structural stability (Figure 3b). As a cathode material for potassium-ion batteries, it displayed outstanding cycling performance, achieving a capacity retention rate of 93% after 1000 cycles at  $200 \text{ mA g}^{-1}$ . However, due to the nature of the wet chemical synthesis methods, PBAs produced by co-precipitation always contain crystallization water and defects.<sup>[52]</sup> To improve the quality of PBAs obtained through precipitation, several enhancement strategies have been proposed, such as adjusting the concentration or temperature to reduce the content of  $[\text{Fe}(\text{CN})_6]$  vacancies and coordinated water.

In summary, PBAs synthesized *via* hydrothermal methods exhibit higher crystallinity and superior electrochemical performance.<sup>[68]</sup> However, due to lower yield and the volatilization of toxic hydrogen cyanide during the production process, this method is primarily limited to laboratory studies focusing on mechanisms and principles. Co-precipitation offers scalable production potential for PBAs. Therefore, current optimization strategies mainly focus on improving the quality of PBAs produced *via* co-precipitation, laying the foundation for the future commercialization of PIBs.

## 4. Optimization Strategies for PBA

To promote the commercialization of PIBs, cathode materials are required to exhibit high energy density, long life, and high-rate performance.<sup>[69]</sup> However, PBA cathodes still suffer several

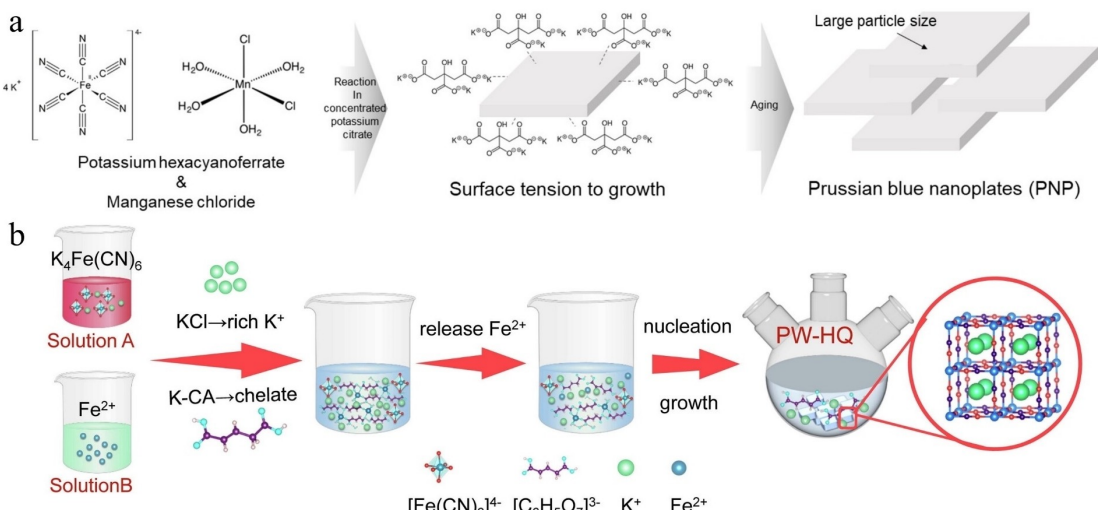


Figure 3. Schematic diagram of the co-precipitation method.<sup>[66,67]</sup> Reproduced with permission.<sup>[66,67]</sup> Copyright 2023–2024, Elsevier, Wiley-VCH.

challenges including structural defects and vacancies, crystalline water, irreversible phase transitions, etc., which will adversely affect the electrochemical performance.<sup>[70]</sup> To address these issues, considerable efforts have been made to synthesis high-quality PBAs, inhibit side reactions or improve structural stability. This section will systematically discuss three optimization strategies to enhance the electrochemical performance of PBAs, including crystal structure regulation, interface regulation and composite materials, which may contribute to the practical application of PBAs.

#### 4.1. Crystal Structure Regulation

##### 4.1.1. Chelating Agent

Typically, high-quality PBAs exhibit the following characteristics: fewer  $\text{Fe}(\text{CN})_6$  vacancies and water molecules, regular cubic morphology, and enhanced thermal stability. To prepare high-quality PBAs, chelating agents are generally used to chelate metal ions and further decrease the precipitation rate of PBAs. Currently, the reported chelating agents mainly include citrate-based salts and ethylenediaminetetraacetic acid dipotassium salt (EDTA-2 K). Among them, potassium citrate is one of the most common chelating agents that retard the reaction process. He et al.<sup>[25]</sup> synthesized medium-sized  $\text{K}_{1.78}\text{Fe}[\text{Fe}(\text{CN})_6]_{0.92} \cdot 0.4\text{H}_2\text{O}$  using a potassium citrate-assisted co-precipitation method. They pointed out that potassium citrate could chelate with transition metal ions, further slowing down the crystallization of  $\text{K}_2\text{Fe}[\text{Fe}(\text{CN})_6]$ . Higher amounts of potassium citrate resulted in the medium-sized materials with larger cubic morphology and size, corresponding to a higher crystallinity degree. Moreover, a slight weight loss of 2–3 wt% was observed during TGA testing conducted at temperatures between 150 and 300 °C, indicating a low content of interstitial water in the lattice structure of as-prepared materials (see Figure 4a). The energy density of the optimized electrode reached up to 500 Wh kg<sup>-1</sup>, with a capacity retention rate of 65% after 300 cycles (see Figure 4b).

In recent years, there has been a tendency to use ethylenediaminetetraacetic acid dipotassium salt (EDTA-2 K) as a chelating agent due to its stronger chelating ability than potassium citrate, resulting in slower nucleation and growth rates of PBAs. Deng et al.<sup>[71]</sup> reported a  $\text{K}_{1.94}\text{Mn}[\text{Fe}(\text{CN})_6]_{0.994} \square_{0.006} \cdot 0.08\text{H}_2\text{O}$  with a negligible content of defects and water utilizing EDTA-2 K as the chelating agent. As shown in Figure 4c, after the addition of EDTA-2 K, the particle size of PBAs increased from 50 to 160 nm, with the decrease of  $\text{Fe}(\text{CN})_6$  vacancies (from 8 to 0.6 wt%) and water (from 7.51 to 0.44 wt%), indicating the significant improvement of crystallinity. From UV-vis spectroscopy results, this can be attributed to the 5-fold extension of the precipitation time of  $\text{K}_4\text{Fe}(\text{CN})_6$  in solution after adding EDTA-2 K, which facilitated the growth of high-quality PBAs (see Figure 4d). When tested in combination with a K metal anode, the low-defect electrode enabled a cell-specific energy of 609.7 Wh kg<sup>-1</sup> and 80% capacity retention after 7800 cycles. Lin et al.<sup>[72]</sup> likewise opted to include EDTA-2 K

during the co-precipitation process to suppress nucleation and growth of PBAs (see Figure 4e). The optimized KPB-2E//graphite full-cell exhibited a high capacity of  $102.4 \text{ mAh g}^{<\text{M}->1}$  at  $100 \text{ mA g}^{-1}$ , superior rate capability ( $40.4 \text{ mAh g}^{-1}$  at  $1500 \text{ mA g}^{-1}$ ) and good cycling stability (88% capacity retention after 400 cycles at  $1000 \text{ mA g}^{-1}$ ). Furthermore, it was argued by Shu et al.<sup>[59]</sup> that most researchers focused on reducing lattice defects and interstitial water, nevertheless, a key parameter of crystal structure, i.e. crystallinity, was urgently worth discussing in order to elucidate the role of dynamic control on the bulk properties of PBAs. They introduced EDTA-2 K during the co-precipitation process and synthesized  $\text{K}_2\text{Fe}[\text{Fe}(\text{CN})_6]$  with high crystallinity and ion diffusion coefficient. The high structural stability of this highly crystalline structure was further confirmed by *in-situ* XRD results (see Figure 4f), which ensured its super-stable cycling performance with 61.3% capacity retention at after 5000 cycles. Wang et al.<sup>[30]</sup> also used EDTA-2 K during the synthesis process of PBAs, while their ultimate objective was to synthesize PBAs with  $\text{Fe}^{\text{III}}$  vacancies through chelating agents. Density Functional Theory (DFT) calculation revealed that  $\text{Fe}^{\text{II}}$  vacancies can inhibit the movement of the Fe–C bond, which contributed to the reduction of lattice distortion in Fe–C octahedron, resulting in the high cyclic stability of PBAs. Finally, the optimized sample displayed a stable discharge capacity of  $40 \text{ mAh g}^{-1}$  at  $100 \text{ mA g}^{-1}$  after 250 cycles (see Figure 4g).

Through the extensive literature review, it is concluded that the nucleation and growth rates of PBAs can be significantly reduced with the addition of chelating agents. Concretely, in the co-precipitation method, the inclusion of potassium chelating agents offers dual benefits: it not only enhances the crystallinity of PBAs but also increases the initial potassium content. This improvement can be attributed to the additional  $\text{K}^+$  supply while reducing the interstitial water. It should be noted that the increase in grain size upon the addition of chelating agents is not entirely beneficial for electrochemical performance. Although the larger PBA framework can provide more  $\text{K}^+$  storage sites, the utilization of the internal active materials may be compromised, leading to rapid capacity decay. In current studies, chelating agents are generally not proposed as a separate strategy. Instead, they are used in conjunction with various other processes to control the size and crystallinity of PBAs.

##### 4.1.2. Potassium Salts Addition

During the material synthesis process, in addition to an appropriate amount of chelating agents, an excess of potassium salts is typically added to increase the concentration of  $\text{K}^+$  in the solution. The currently reported potassium salts mainly include KCl and KI, which facilitate the preparation of PBAs with low defects and high potassium content, ensuring a higher specific capacity and more stable cycle performance for the final electrochemical performance. For example, Zhou et al.<sup>[73]</sup> utilized the relatively uncommon KI to synthesize spindle-shaped PW ( $\text{K}_{1.72}\text{Fe}[\text{Fe}(\text{CN})_6]_{0.96} \cdot 0.342\text{H}_2\text{O}$ ), which provided abundant active sites and reduced ion diffusion paths (Fig-

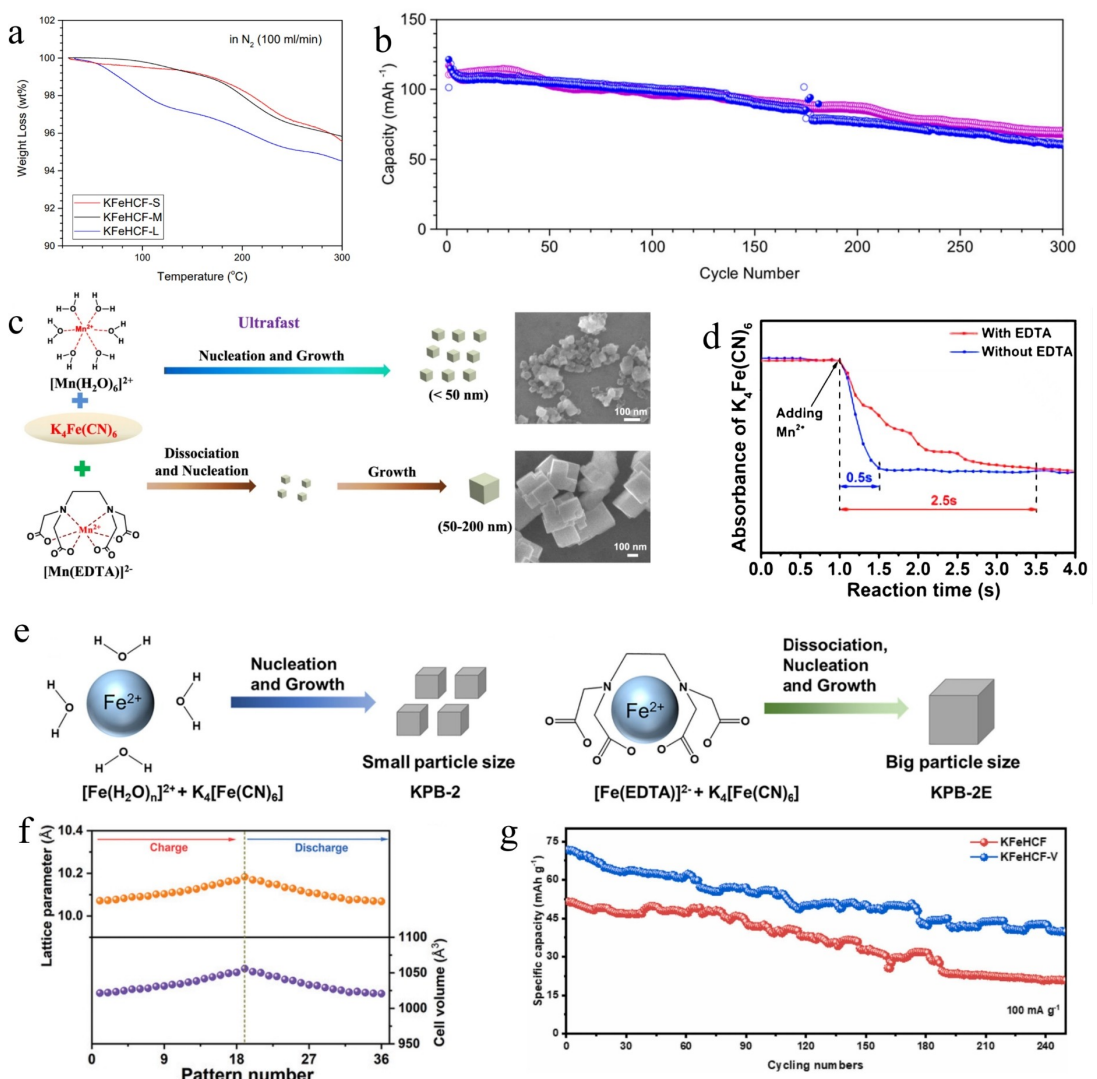


**Figure 4.** a) TGA analysis of the three KFeHCF samples at a scan rate of 5 °C/min.<sup>[25]</sup> b) Cycling performance of the optimized electrode over 300 cycles.<sup>[25]</sup> c) Co-precipitation reaction with or without chelating agent.<sup>[71]</sup> d) *In-situ* UV-vis spectra monitoring the absorption intensity of  $K_4[Fe(CN)_6]$  at 327 nm upon adding  $Mn^{2+}$  aqueous solution with or without the EDTA.<sup>[71]</sup> e) With or without the use of EDTA-2 K chelating agent.<sup>[72]</sup> f) The changes of KFeHCF-E lattice parameter and cell volume calculated by *in-situ* XRD.<sup>[59]</sup> g) Long-term cycling performance of KFeHCF and KFeHCF-V at 100 mA g<sup>-1</sup>, which have been activated after 5 cycles at 25 mA g<sup>-1</sup>.<sup>[30]</sup> Reproduced with permission.<sup>[25,30,59,71,72]</sup> Copyright 2017–2023, Elsevier, American Chemical Society, Wiley-VCH.

ure 5a). Theoretical calculations showed that the irregular PW ( $[Fe[Fe(CN)]_{6,0.89} \cdot 0.89H_2O$ ) synthesized without KI had higher defect content. The high potassium content, low defect, and low water content in the spindle-shaped PW ensured its high specific capacity and stable cycling performance, achieving a reversible capacity of 124.2 mA h g<sup>-1</sup>, an operating voltage platform of 3.32 V, and a capacity retention of 89.2% after 500 cycles. Additionally, the construction of the spindle-shaped layered porous structure significantly accelerated potassium ion transport within the electrode materials, greatly enhancing its rate performance (see Figure 5b). Zhao et al.<sup>[26]</sup> synthesized potassium-rich mesoporous nickel ferricyanide ( $K_2NiFe(CN)_6 \cdot 1.2H_2O$ ) using the commonly used KCl. They found that the addition of KCl during the co-precipitation process resulted in uniform and smaller particle size distributions of PBAs. These nanoblocks with diameters ranging from 10 to 20 nm sponta-

neously aggregated into uniform NiFC-porous materials during co-precipitation. The pore size distribution curve confirmed that the mesoporous structure had large channel sizes, supporting rapid potassium ion insertion/extraction with minimal volume change (7.7%), and a capacity retention of 98.6% after 5000 cycles (Figure 5c).

#### 4.1.3. Transition Metal Ions Doping

Recently, it is found that transition metal ions doping or substitution can promote the electrochemical properties of PBAs such as capacity, voltage, rate and cyclability. According to the different physicochemical properties of metal ions, the chemical composition of PBAs can be adjusted by doping without destroying the crystal structure, resulting in the

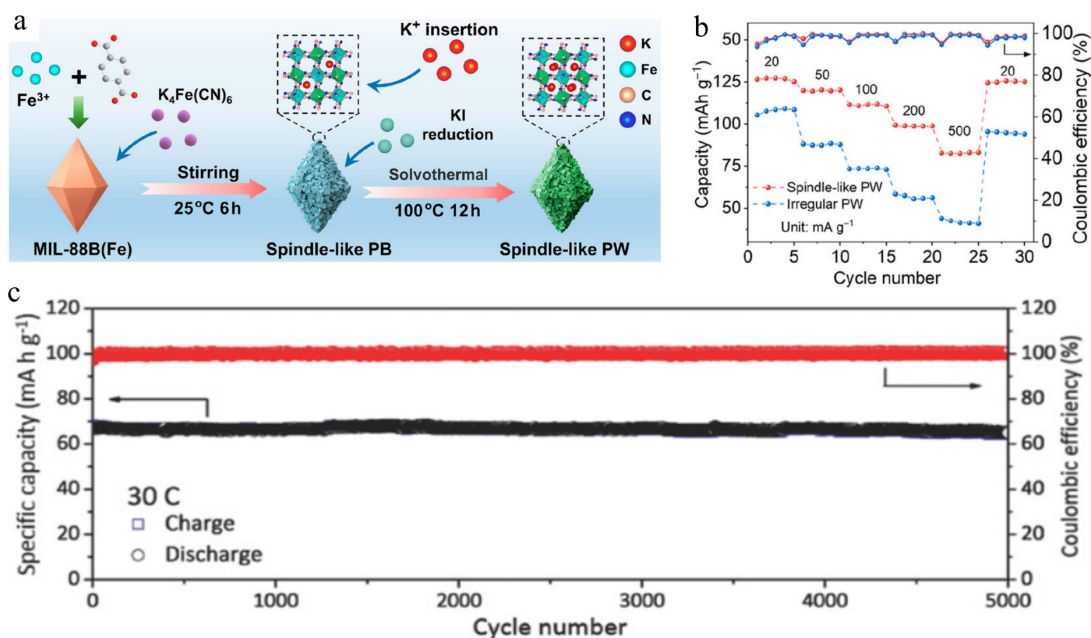


**Figure 5.** a) Schematic illustration of the formation procedure of spindle-like PW.<sup>[73]</sup> b) Rate capabilities of spindle-like PW and irregular PW.<sup>[73]</sup> c) Long-term cycling performance at 30 C.<sup>[26]</sup> Reproduced with permission.<sup>[26,73]</sup> Copyright 2018–2023, American Chemical Society, Wiley-VCH.

structural diversity. Therefore, single and multi-transition metal doped PBAs with different properties have been synthesized according to the needs of practical applications. Table 1 shows the summary of representative transition metal doped PBA cathodes in current PIBs. For example, Gao et al.<sup>[74]</sup> discovered that Mn-PBAs exhibited high redox potentials, but their potassium storage capacity significantly decreased over cycling. Instead, Fe-PBAs displayed good cycle stability, albeit with lower redox potentials. Therefore, they synthesized Fe/Mn co-doped PBAs, which not only exhibited a high average discharge voltage (3.82 V vs. K<sup>+</sup>/K), but also possessed excellent cycle stability (90 mAh g<sup>-1</sup> after 600 cycles). These results indicated that the co-doped coordination structure can enhance the redox potential of N-coordinated Fe and increase the capacity contribution at high voltages (above 3.5 V) (see Figure 6a). Additionally, the co-doped structure can effectively suppress the dissolution of transition metal ions which maintained the electrode structural integrity during insertion/extraction processes, thus ensuring outstanding cycle stability. Analogously, Chen et al.<sup>[75]</sup> employed Fe substitution in Mn-PBAs, which revealed that Fe substitution can stabilize the lattice structure and reduce the Mn Jahn-Teller distortion of Mn<sup>3+</sup>, thereby limiting material transition only between monoclinic and cubic phases during charge and discharge processes. However, with increasing iron content, vacancy defects and crystalline water also increased, thereby compromising the integrity of the crystal structure and deteriorating the electrochemical performance. The final results indicated that the electrochemical performance of the sample with 10% Fe substitution was optimal, providing a high reversible capacity of 124.3 mAh g<sup>-1</sup> with a capacity retention of 70.0% after 200 cycles at 100 mA g<sup>-1</sup>. Except Mn-based PBAs, Fe ion substitution had

proved effective on other PBAs systems. Wang et al.<sup>[76]</sup> employed a room-temperature co-precipitation method to carry out *in-situ* Fe substitution in Co-PBAs, resulting in the preparation of K<sub>1.66</sub>Fe<sub>0.25</sub>Co<sub>0.75</sub>[Fe(CN)<sub>6</sub>] · 0.83H<sub>2</sub>O with low water content, high crystallinity, and a high potassium ion diffusion coefficient (see Figure 6b). After 400 cycles at 100 and 200 mA g<sup>-1</sup>, approximately 97% and 90.6% discharge capacity retentions were obtained, respectively, demonstrating the high reversibility and structural stability of optimized electrodes.

The substitution of Ni is widely used as a potent strategy to enhance the structural stability of PBAs. Huang et al.<sup>[77]</sup> reported the optimization of electrochemical performance for PBAs by doping with different proportions of Ni. They found that PB doped with 5% Ni, namely K<sub>2</sub>Ni<sub>0.05</sub>Fe<sub>0.95</sub>Fe(CN)<sub>6</sub>, exhibited the best electrochemical performance, with capacity retention of 83.1% after 300 cycles at 0.1 A g<sup>-1</sup> (see Figure 6c). More importantly, the discharge capacity at the high voltage plateau increased from ~40 up to 53 mAh g<sup>-1</sup>, ensuring a higher energy density of PIBs. Characterization results revealed that doping with a suitable amount of Ni ions could activate the C-coordinated Fe<sup>2+</sup>C<sub>6</sub>/Fe<sup>3+</sup>C<sub>6</sub> redox reaction by changing the electronic state of the Fe ions, thus facilitating the diffusion of K ions during charging and discharging. Liao et al.<sup>[61]</sup> synthesized a series of ternary K<sub>2</sub>Ni<sub>x</sub>Co<sub>1-x</sub>Fe(CN)<sub>6</sub> compounds with various Co/Ni ratios for potassium-ion storage (see Figure 6d). By optimizing PBAs with Ni and Co connected to the N end, which could balance the structural disturbances during potassiation/depotassiation, the ternary K<sub>2</sub>Ni<sub>0.36</sub>Co<sub>0.64</sub>Fe(CN)<sub>6</sub> exhibited superior performance compared to its binary counterparts (see Figure 6e). It was found that the ternary K<sub>2</sub>Ni<sub>0.36</sub>Co<sub>0.64</sub>Fe(CN)<sub>6</sub> had a high initial capacity of 86 mAh g<sup>-1</sup> and a high capacity retention of 98% after 50 cycles at 20 mA g<sup>-1</sup>, which surpassed

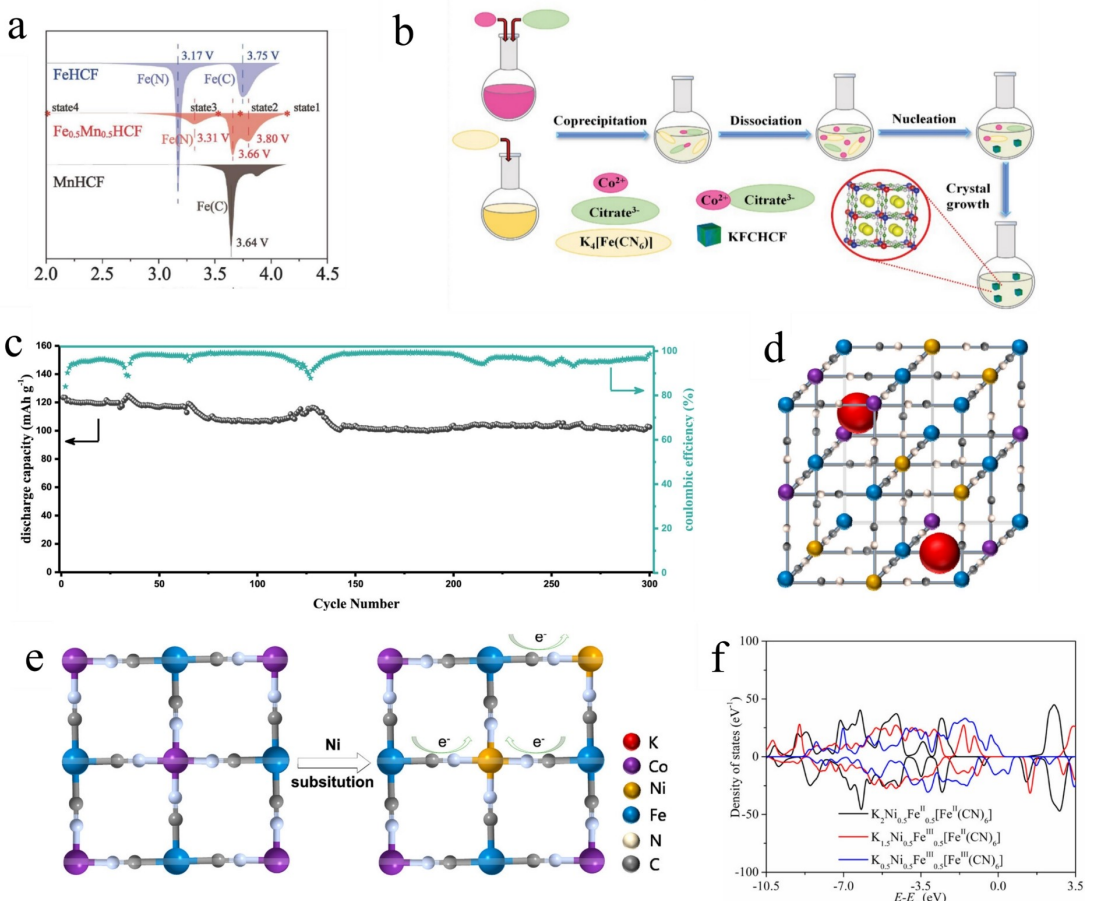


**Figure 6.** a) Diagram: three reduction parts of MnHCF, FeHCF and  $\text{Fe}_{0.5}\text{Mn}_{0.5}\text{HCF}$  CV curves.<sup>[74]</sup> b) Schematic demonstration of the coprecipitation process to synthesize the KFHCF sample.<sup>[76]</sup> c) Long-cycling test of NiFePB-5 sample at a current density of 100 mA g<sup>-1</sup>.<sup>[77]</sup> d) Mechanism schematic of Ni substitution.<sup>[61]</sup> e) Crystal structure of the  $\text{PBN}_x\text{C}_{1-x}$  sample.<sup>[61]</sup> f) DOS of KNFHCF-1/2 at different charging states.<sup>[27]</sup> Reproduced with permission.<sup>[27,61,74,76,77]</sup> Copyright 2019–2024, Elsevier, American Chemical Society, Wiley-VCH.

pure  $\text{K}_2\text{CoFe}(\text{CN})_6$  and  $\text{K}_2\text{NiFe}(\text{CN})_6$ . Liu et al.<sup>[27]</sup> reported the synthesis of PBAs with various nickel contents ( $\text{K}_2\text{Ni}_x\text{Fe}_{1-x}[\text{Fe}(\text{CN})_6]$ ) via a one-step hydrothermal method. As the  $x$ -value increased, i.e., the nickel content increased, the specific surface area and volume of PBA increased. This not only facilitated the efficient storage and diffusion of  $\text{K}^+$  ions, but also provided adequate space to buffer the volume strain during charge/discharge processes. Compared to KNFHCF without Ni substitution, KNFHCF-1/2 ( $\text{K}_{1.9}\text{Ni}_{0.5}\text{Fe}_{0.5}[\text{Fe}(\text{CN})_6]_{0.89} \cdot 0.42\text{H}_2\text{O}$ ) exhibited superior cycling stability. After 200 cycles, KFHCF suffered severe capacity decay with a capacity retention of 69.0%, whereas KNFHCF-1/2 exhibited a much higher capacity retention of 96.3% after 200 cycles. Furthermore, DFT calculations showed that in the fully charged state, the valence state of KNFHCF-1/2 crossed the Fermi level more than that of KFHCF, implying that KNFHCF-1/2 was a metallic system, which led to faster potassium storage kinetics (see Figure 6f). In summary, it could be concluded that the introduction of inert Ni ions linked through N atoms could reduce the band gap, the  $\text{K}^+$  diffusion activation energy, and the formation energy of the charged state, thus resulting in the optimal performance of KNFHCF-1/2.

Overall, PBAs based on different transition metal possess different advantages. For example, the most common Fe-PBA exhibits high capacity and superior cycling stability, while Mn-PBA offers a high theoretical capacity as well as high working voltage. In addition, Ni-PBA generally undergoes smaller volume changes during  $\text{K}^+$  insertion/extraction, which contributes to more stable cycling performance. However, each type of transition metals has its own limitations. Therefore, considering the factors of cost, inherent structural characteristics and electrochemical performance, the practical application of multi-metal doped PBAs in PIBs shows significant potential. Recently, the use of high-entropy PBAs (HE-PBAs) has gained popularity in SIBs,<sup>[79–82]</sup> and the concept and research of HE-PBAs in PIBs hold great promise and warrant further investigation.<sup>[83]</sup> At present, Ma et al.<sup>[84]</sup> have synthesized a high-entropy PBA using five different transition metals, and the obtained sample exhibited significant electrochemical stability. Compared with traditional PBAs, HE-PBAs possess superior thermodynamic stability and enhanced ion migration kinetics. In the near future, this work will lay the foundation for the development of more excellent high-entropy materials in PIBs.

#### 4.1.4. Other Optimization Strategies

Except for the above-mentioned optimization strategies, some other methods have also been identified to effectively reduce lattice defects and ultimately synthesize PBAs with high crystallinity. For instance, Ma et al.<sup>[85]</sup> introduced an electrostatic field during the co-precipitation process, thereby enhancing the crystallinity of PBAs (see Figure 7a). This electrostatic atomization technique resulted in the synthesis of a potassium-rich  $K_{1.86}Ni[Fe(CN)_6]_{0.87}\square_{0.13}\cdot 1.88H_2O$ . Moreover, the microstructure was optimized by the influence of electrostatic repulsion, leading to an enhanced electrochemical activity. Compared to the sample without electrostatics, the potassium-rich electrode displayed a significant enhancement of electrochemical performance. Dong et al.<sup>[86]</sup> focused on studying the inert atmosphere during the co-precipitation process. Instead of the use of an inert atmosphere, they utilized the chemical reaction between iron powder and excess citric acid to spontaneously generate hydrogen gas during synthesis (see Figure 7b), followed by the reaction between ferrocyanide and  $Fe^{2+}$  ions to form PBA powder. The hydrogen gas could effectively protect

the prepared PBA from oxidation by increasing the internal pressure within the reaction vessel. The resulting sample, namely  $K_{1.62}Fe[Fe(CN)_6]_{0.92}\cdot 0.33H_2O$ , exhibited a high capacity of  $120.9\text{ mA h g}^{-1}$  at  $50\text{ mA g}^{-1}$  and maintained a high capacity retention of 98.2% after 100 cycles (see Figure 7c).

Recently, Wang et al.<sup>[32]</sup> proposed a novel thermal restoration method for surface vacancies, where sodium citrate was introduced as reductant at high temperatures. Under this method,  $Fe^{III}(CN)_6$  in the precursor lattice was gradually reduced to  $Fe^{II}(CN)_6$ . Subsequently,  $Fe(CN)_6^{4-}$  ions in the solution gradually entered the PBAs framework and filled the  $Fe(CN)_6$  vacancies surface, which effectively repaired surface vacancies (Figure 7d). The product obtained at high temperature ( $90^\circ C$ ), KMHCF-H ( $K_{1.82}Mn[Fe(CN)_6]_{0.98}\cdot [Fe(CN)_6]_{0.02}\cdot 0.58H_2O$ ), exhibited an initial discharge capacity of  $108\text{ mAh g}^{-1}$ , along with high capacity retention of approximately 95% after 2000 cycles at 1 C. It is found that the low content of  $Fe(CN)_6$  vacancies on the KMHCF-H surface allowed the preferential decomposition of Potassium Bis(fluorosulfonyl)imide (KFSI) in the electrolyte, thereby forming a dense anion-dominated cathode electrolyte

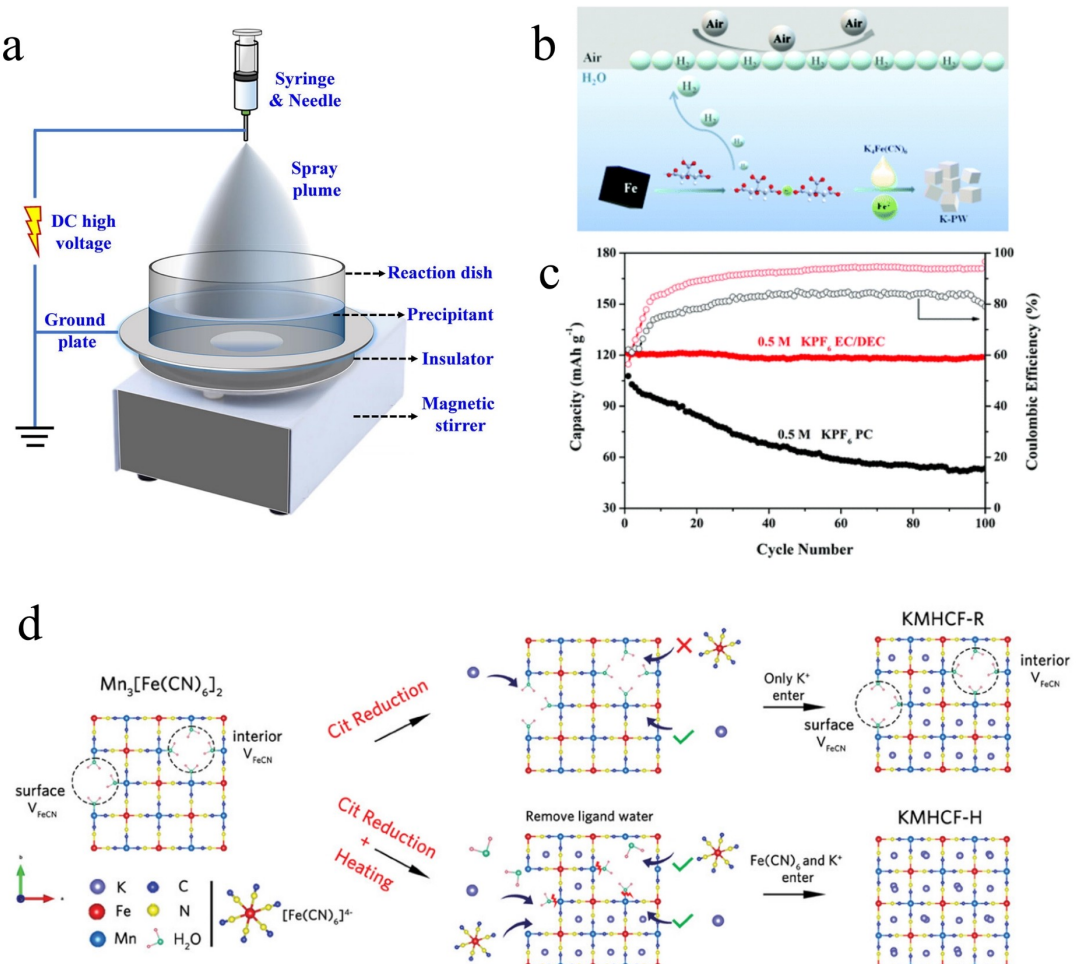


**Figure 7.** a) Schematic diagram of the program.<sup>[85]</sup> b) Schematic of the synthesis route with autogenous gas protection.<sup>[86]</sup> c) The cycling performance in different electrolytes at a current density of  $50\text{ mA g}^{-1}$ .<sup>[86]</sup> d) Schematic illustration of different reaction processes with or without thermo-induction.<sup>[32]</sup> Reproduced with permission.<sup>[32,85,86]</sup> Copyright 2019–2024, Elsevier, Royal Society of Chemistry, Wiley-VCH.

interface (CEI), which effectively suppressed Mn dissolution into the electrolyte.

## 4.2. Interface Regulation

In addition to the effects of the intrinsic crystal structure, various other detrimental factors have been confirmed effective for the electrochemical properties of PBAs. Among them, the interface issues of PBAs are particularly pervasive. During cycling, the consumption of the electrolyte on the anode side leads to the formation of solid-electrolyte interface (SEI) films. An unstable SEI film continuously consumes the electrolyte, ultimately resulting in interface side reactions and electrode failures. Therefore, establishing a stable interface is crucial for constructing high-performance PBAs electrodes in PIBs.

### 4.2.1. Surface Coating Technology

Surface coating technology can effectively alleviate the interface problems by wrapping the inorganic compounds or carbon

materials on the surface of PBAs as a protective layer. However, as mentioned earlier, the structure of PBAs is easily degraded at high temperatures. Consequently, the common carbon coating method cannot be applied on the surface modification of PBAs owing to the high pyrolysis temperatures of carbon sources. This significantly limits the selection of coating strategies, and suitable conductive coating materials must be chosen at a low temperature, including polydopamine, poly(3,4-ethylene dioxythiophene). Xue et al.<sup>[87]</sup> utilized a Polypyrrole (PPy) conductive coating to protect PBA materials (see Figure 8a). In this

study, pyrrole was *in-situ* polymerized on the PBA surface through the intrinsic oxidizing ability of PBA, eliminating the addition of oxidizing agent. The introduction of this conductive polymer could enhance the electronic conductivity of PBA, thereby improving its rate performance. As a result, the PBA@PPy electrode exhibited a high discharge capacity of  $72.1 \text{ mAh g}^{-1}$  at a current density of  $1000 \text{ mA g}^{-1}$ , which slightly decreased to  $61.8 \text{ mAh g}^{-1}$  after 500 cycles (see Figure 8b), corresponding to a capacity decay rate of only 0.03% per cycle. Moreover, *ex-situ* XRD combined with DFT calculations indicated that  $\text{K}^+$  storage in PBA@PPy was related to a reversible interaction mechanism without phase trans-

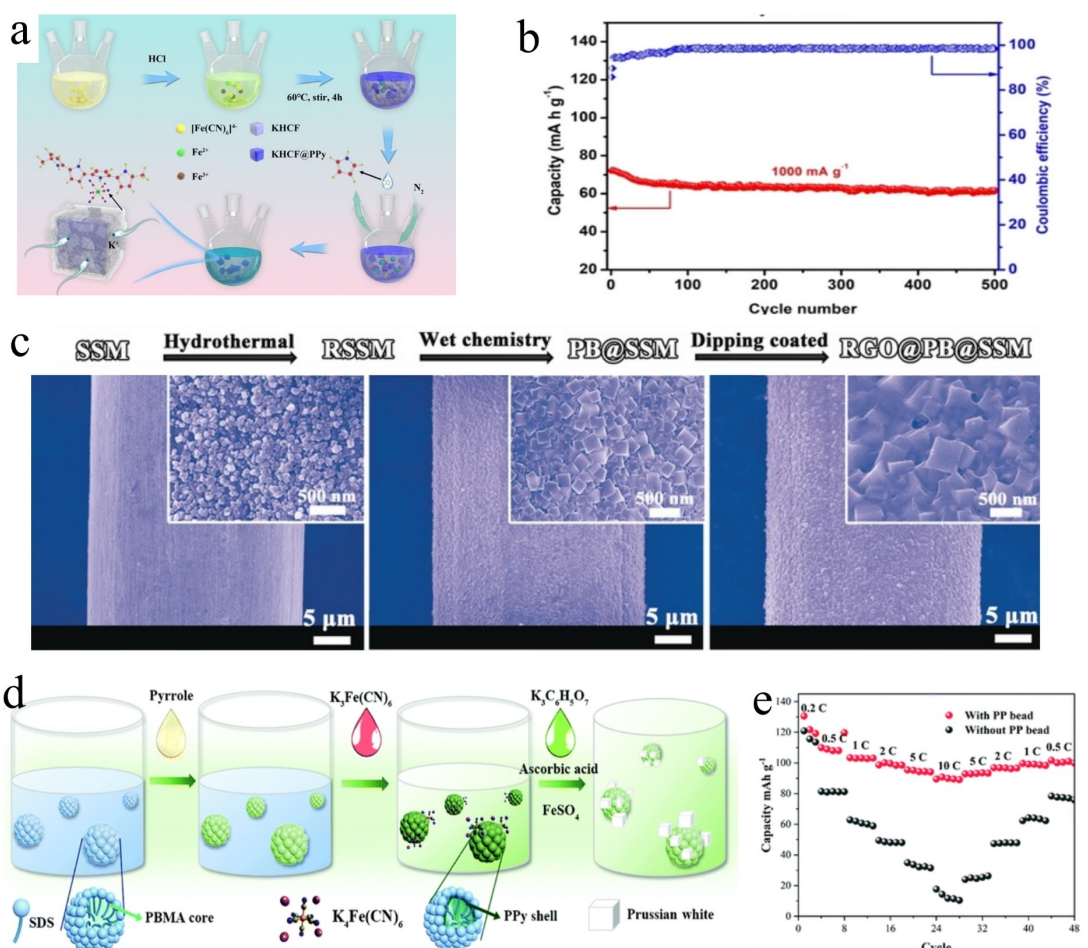


**Figure 8.** a) Pure KHCF and KHCF@PPy: Illustration scheme of the synthesis process.<sup>[87]</sup> b) Long cycling performance at  $1000 \text{ mA g}^{-1}$ .<sup>[87]</sup> c) SEM images of RSSM, PB@SSM, and RGO@PB@SSM.<sup>[88]</sup> d) Synthesis of KFeHCF sample with PP bead: schematic illustration of the *in-situ* synthesis.<sup>[89]</sup> e) Rate performance of two samples of KFeHCF.<sup>[87-89]</sup> Reproduced with permission.<sup>[87-89]</sup> Copyright 2017–2020, American Chemical Society, Wiley-VCH, Royal Society of Chemistry.

formation, which was beneficial for the structural stability. Additionally, it has been mentioned earlier that the major issue of Mn-PBAs is the dissolution of manganese under high voltage conditions, leading to the capacity decay. Once manganese dissolves into the electrolyte,  $Mn^{2+}$  ions would deposit on the anode surface, followed by disrupting the solid electrolyte interface, accelerating electrolyte decomposition, and blocking ion transport pathways, which eventually results in the capacity loss. Conventional surface coating approaches have been shown to decrease the capacity and discharge voltage of Mn-PBAs, thus sacrificing the energy density. Zhu et al.<sup>[88]</sup> employed rusty stainless steel meshes as an iron source to convert the corrosion layer into compact stack layers of Prussian blue nanocubes (PB@SSM). To further enhance the conductivity and improve the structural stability of the PB@SSM electrode, a layer of reduced graphene oxide (rGO) was also coated on its surface (see Figure 8c). As a result, this unique RGO-coated structure displayed a high capacity of  $96.8 \text{ mAh g}^{-1}$ , a high voltage of 3.3 V, and a high rate performance of  $35 \text{ mAh g}^{-1}$  at a current density of  $1000 \text{ mA g}^{-1}$ . Chen et al.<sup>[89]</sup> reported a nanosized organogel, namely poly(butyl methacrylate) (PBMA), showing high binding strength and fast absorption capability with multiple electrolytes. This PBMA polymer simultaneously worked as a coating layer and an adhesive conducting organogel for connecting precipitated PBA nanoparticles internally. Especially, the obtained cross-linked PBMA nano-beads can absorb multiple electrolyte solvents within 3 seconds from the dried state, and then converts to an organogel, as a moisturizer and extra-binder (see Figure 8d). Therefore, the introduction of PBMA can effectively solve the powder falling problem of electrodes, and hence the electrochemical performance of PBAs was greatly improved, with an initial discharge capacity of  $130 \text{ mAh g}^{-1}$  at 0.2C, a discharge capacity of  $90 \text{ mAh g}^{-1}$  at 10 C (see Figure 8e), and a high capacity retention of 82% after 300 cycles.

In summary, it can be observed that surface coating technology serves dual purposes: a protective layer to prevent the dissolution of electrode materials during cycling and an electronic conductor to enhance the electronic conductivity of PBAs. Therefore, the PBA electrodes with surface coating generally exhibit enhanced cycling stability and rate performance. In order to promote the commercialization of PBAs, the future research should concentrate on identifying cost-effective and efficient coating sources.

#### 4.2.2. Cathode-electrolyte Interface Regulation

The stability of electrode-electrolyte interfaces is not only related to the surface of the electrode, but also closely associated with the properties of the electrolyte. The composition of the electrolyte determines the properties of the SEI films which formed by the reduction reaction occurring at the solid-liquid interface on the surface of PBAs. Additionally, the electrochemical stability of the electrolyte dictates the operating potential range of the battery, while the thermal stability of the battery also depends on the composition of the

electrolyte.<sup>[90–93]</sup> Currently, the electrolytes used in potassium batteries primarily consist of KFSI or potassium hexafluorophosphate (KPF<sub>6</sub>) combined with solvents such as triethyl phosphate (TEP), 1,2-Dimethoxyethane (DME), ethylene carbonate (EC), diethyl carbonate (DEC), and dimethyl carbonate (DMC). Guo et al.<sup>[94]</sup> first proposed the KFSI/TEP electrolyte formulation for PIBs. By increasing the concentration of the main salt (KFSI) to 2 M, they achieved stable cycling performance for the potassium storage. This electrolyte exhibited advantages such as low cost, low viscosity, and high conductivity. Furthermore, it enabled the formation of a uniform and robust salt-based SEI layer. Moreover, during the study of electrolyte systems for lithium and sodium ion batteries, it was found that the instability at the cathode-electrolyte interface can be resolved using liquid electrolyte additives. Zhang et al.<sup>[95]</sup> introduced a saturated potassium nitrate (KNO<sub>3</sub>) additive in the 2 M KFSI/TEP electrolyte, which altered the surface charge distribution and effectively suppressed the decomposition of KFSI on high-voltage cathodes (see Figure 9a). Differential capacitance tests revealed that the minimum point of the capacitance curve (located at 2.3 V in the nitrate-free electrolyte) shifted to 2.18 V with the addition of nitrate, which indicated that the addition of nitrate may affect the electrical double layer (EDL) structure. Furthermore, electrochemical quartzcrystal microbalance (EQCM) technology detected that the transition voltage of the nitrate-containing electrolyte (2.30 V) was 0.17 V lower than that of the nitrate-free electrolyte (2.47 V).

This observation also confirmed that nitrate altered the surface charge distribution. The nitrate-free electrolyte was found to be unstable at 4.3 V with very limited cycling (up to the 15th cycle), indicating the poor high-voltage tolerance. In contrast, the nitrate-containing electrolyte demonstrated impressive cycling stability, lasting over 8 months (more than 2800 cycles) with a capacity retention rate of 66% (80% capacity retention after 2048 cycles). Another example is the introduction of fluorinated solvents, which could weaken the interactions between metal cations and solvents without affecting the conductivity of the material. FEC is a common passivation enhancer used to suppress side reactions between K metal and the electrolyte. Jiang et al.<sup>[96]</sup> tested  $K_{1.6}Mn[Fe(CN)_{6}]_{0.96} \cdot 0.27H_2O$  (KMFC) with various electrolyte formulations including 1 M KFSI in EC/DEC, EC/DEC/FE and PC/FEC.

As shown in Figure 9b, after adding 10 wt % FEC, the potassium metal lost its silver luster, indicating that a certain degree of passivation had occurred on the metal surface. As evident from the electrochemical test results, the polarization significantly decreased, and the Coulombic efficiency increased to 92% after the addition of FEC (see Figure 9c-d). This demonstrated that FEC can establish a stable and electrochemically active passivation layer on the potassium surface. Luo et al.<sup>[97]</sup> chose to enhance the electrochemical stability by adding KSeCN to the conventional carbonate electrolyte to construct a stable and conductive CEI films. XRD patterns and ICP-OES measurements indicated that (see Figure 9e-f) KSeCN can significantly improve electrode stability by effectively suppressing side reactions. The derived CEI effectively prevented the dissolution of Fe from the cathode structure.

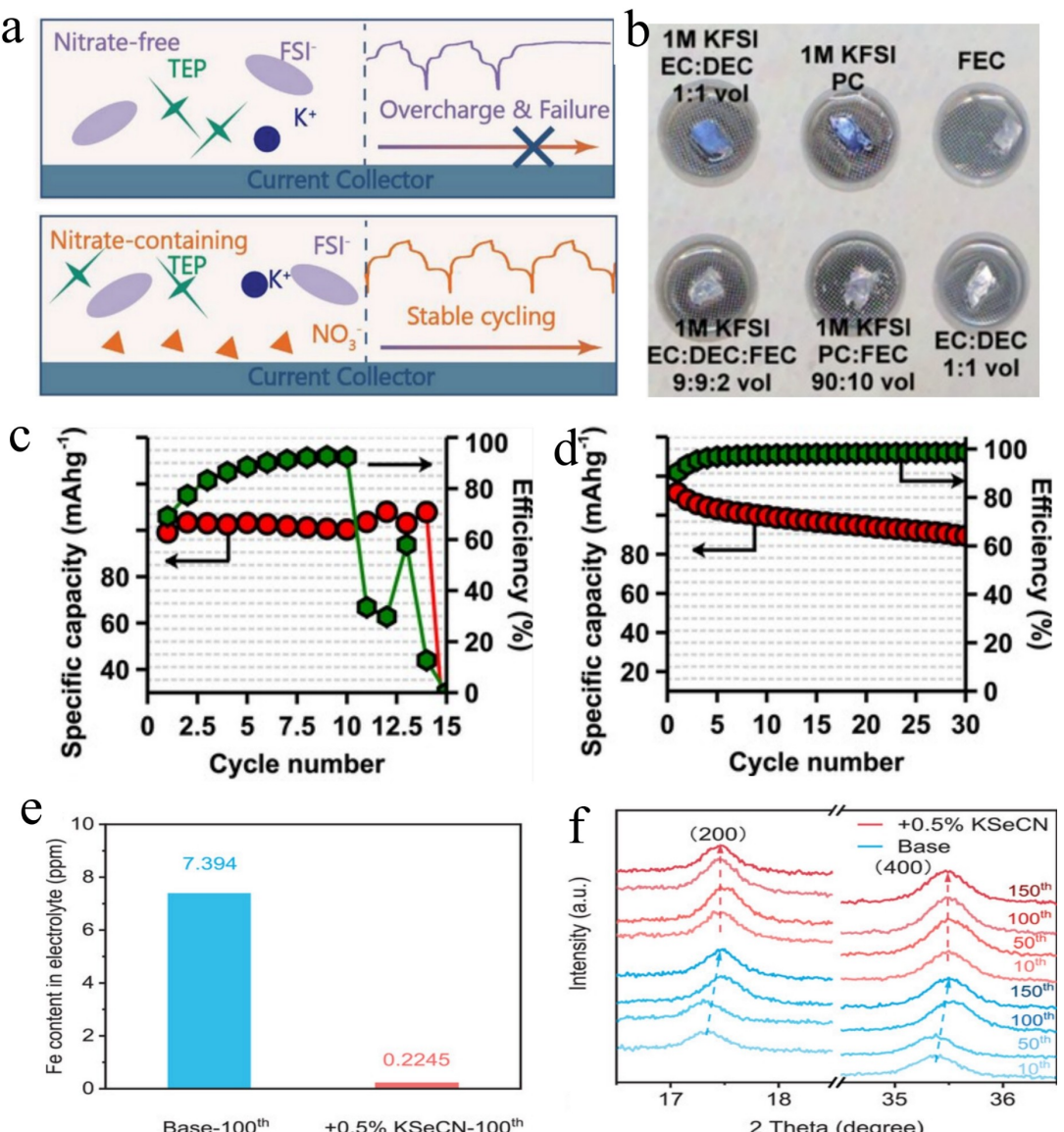


**Figure 9.** a) The scheme of interface at cathode in nitrate-free and nitrate-containing electrolytes.<sup>[95]</sup> b) Reactions of potassium metal in different electrolytes.<sup>[96]</sup> c) Capacity retention and coulombic efficiency (EC:DEC).<sup>[96]</sup> d) Capacity retention and Coulombic efficiency (EC:FEC).<sup>[96]</sup> e) ICP-OES analysis of base and modified electrolytes in K||KFeHCF batteries at 100 cycles.<sup>[96]</sup> f) Ex-situ XRD patterns of KFeHCF cathode at different number of cycles in K||KFeHCF batteries with base and modified electrolytes.<sup>[97]</sup> Reproduced with permission.<sup>[95-97]</sup> Copyright 2017–2024, Royal Society of Chemistry, Wiley-VCH.

Furthermore, the K||KFeHCF battery maintained a high capacity retention rate of up to 87% after 500 cycles, far exceeding that of the baseline electrolyte (27%).

#### 4.3. Composite Materials

Besides coating modification on the surface of PBAs, designing composite structures formed by carbon materials and PBAs is also an effective strategy. This approach can enhance the electronic conductivity of PBAs by providing nucleation sites on the carbon substrate or removing crystalline water, thereby reducing Fe(CN)<sub>6</sub><sup>4-</sup> vacancies and water content, and even achieving a high-quality bulk phase.<sup>[98]</sup> Wei et al.<sup>[99]</sup> addressed

the issues of low electronic conductivity and framework defects in PB that deteriorate electrochemical performance by compositing PB with conductive rGO. During the composite formation, the loss of oxygen-containing functional groups on the rGO substrate weakened the interaction between PB and rGO, resulting in poor electrochemical performance of the PB/rGO composite. To overcome this issue, they utilized polyvinylpyrrolidone (PVP) to directly link PB and rGO (PB/PVP-rGO) (see Figure 10a). The long-chain polymer PVP, through its amide groups, facilitated the complexation with rGO, enhancing the dispersion of rGO in solution. The PB/PVP-rGO composite exhibited excellent rate performance and cycling stability, highlighting the effective interaction between PB and the rGO substrate facilitated by the PVP bridge. Additionally, Zhang

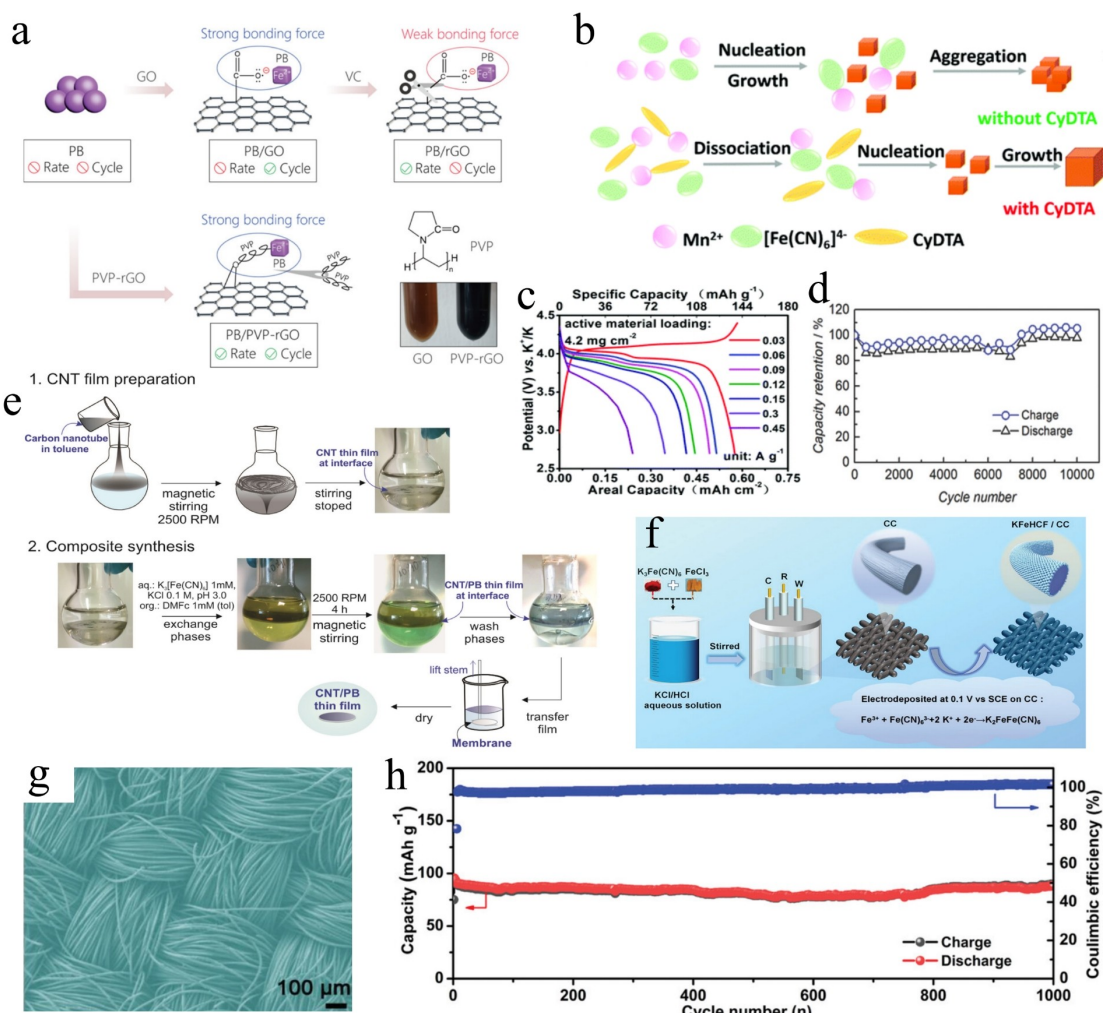


**Figure 10.** a) Experimental steps to prepare CNT/PB thin films at L/L interface.<sup>[99]</sup> b) Schematic illustration of the fabrication of  $K_2Mn[Fe(CN)_6]$  without or with the chelating agent CyDTA.<sup>[100]</sup> c) Rate capability tested under a constant charge specific current of  $30 \text{ mA g}^{-1}$  (0.2 C).<sup>[100]</sup> d) Capacity retention in 10 000 charge/discharge cycles.<sup>[103]</sup> e) Preparation Processes and Interaction States of PB/GO, VC-Reduced PB/rGO, and PVP-Modified PB/PVP-rGO.<sup>[102]</sup> f) Schematic illustration of the synthesis and formation mechanism of KFeHCF/CC by electrodeposition.<sup>[104]</sup> g) Low-magnification SEM images of the as-prepared KFeHCF/CC.<sup>[104]</sup> h) Long-term cycling stability of the K-rich KFeHCF/CC electrode at  $500 \text{ mA g}^{-1}$ .<sup>[104]</sup> Reproduced with permission.<sup>[99,100,102–104]</sup> Copyright 2018–2024, Elsevier, American Chemical Society, Electrochemical Society, Wiley-VCH.

et al.<sup>[100]</sup> synthesized  $K_2Mn[Fe(CN)_6]_{0.982}\square_{0.018}0.164\text{H}_2\text{O}$  (KMF) with extremely low defect content by using CyDTA as a chelating agent during the co-precipitation process (see Figure 10b). Subsequently, the material was ball-milled with reduced graphene oxide (RGO) to enhance its electronic conductivity. Benefiting from the robust structural integrity of the low-defect KMF and the high electronic conductivity provided by RGO, the obtained KMF-RGO composite displayed stable cycling performance (no capacity decay during the tested 100 cycles at 0.1 C) and outstanding rate capability (42% capacity retained at 3 C in comparison to 0.2 C) as a cathode material for PIBs when tested under a high active material loading (see Figure 10c). Edson Nossol et al.<sup>[101]</sup> prepared carbon nanotube/PB flexible transparent films as the cathodes utilizing carbon nanotubes as the conductive matrix. The flexible energy storage device maintained 74% of its capacity after 1,000 cycles, showing remarkable structural stability. Husmann

et al.<sup>[102]</sup> employed a classic synthesis method, wherein cubic Prussian blue crystals were selectively grown on the walls of carbon nanotubes, enhancing the interaction between ionic and electronic conductive components. Self-assembled films composed of PBAs and carbon nanotubes were formed at the liquid/liquid interface and transferred onto a flexible membrane to constitute a button cell with an active carbon cathode (see Figure 10e). Under the current density of  $250 \text{ mA g}^{-1}$ , the cell exhibited a capacity of  $47.6 \text{ mAh g}^{-1}$  and an energy density of  $33.75 \text{ Wh kg}^{-1}$ .

Apart from carbon materials, it had been demonstrated that the combination of certain other materials with PBAs can also enhance their potassium storage performance. Coronado et al.<sup>[103]</sup> introduced a direct method for the preparation of PB/MoS<sub>2</sub>-based nanocomposites. MoS<sub>2</sub> provided a two-dimensional active support for the homogeneous nucleation of porous PB nanocrystals, resulting in a superior specific surface area

compared to other methods and producing a compact PB shell covering the entire flake. The PB/MoS<sub>2</sub> composite shown a specific capacity of 215 mAh g<sup>-1</sup> at 1000 mA g<sup>-1</sup>, with a capacity retention rate of up to 90% after 10,000 cycles (see Figure 10d). Finally, while the feasibility of preparing PBAs using electro-deposition has been mentioned earlier, no related research results have been published in the context of PIBs as of the time of writing. Recently, Li et al.<sup>[104]</sup> have utilized the existing potassium-rich ferrocyanide (KFeHCF) and deposited it onto commercial carbon cloth (CC) through an electrochemical deposition method, resulting in the formation of KFeHCF/CC nanocomposites (see Figure 10f). Scanning electron microscopy (SEM) images indicated that potassium ferrocyanide was completely and uniformly covered on the CC (see Figure 10g). This innovative binder-free cathode not only provided a continuous conductive pathway for electrons but also accelerated the diffusion of potassium ions through the active electrode-electrolyte interface. The results demonstrated that its half-cell exhibited a reversible discharge capacity of 110.1 mAh g<sup>-1</sup> after 100 cycles at a current density of 50 mA g<sup>-1</sup>, and a capacity retention rate of 92.3% after 1000 cycles at a current density of 500 mA g<sup>-1</sup> (see Figure 10h).

## 5. Conclusion and Perspective

- (1) The rise and development of PIBs have brought about numerous opportunities for PBAs, which serve as intercalation-type cathode materials, while also posing unprecedented challenges. This review delves into the crystal structure of PBAs and their underlying charging/discharging mechanisms. Furthermore, various strategies for optimizing the electrochemical performance of PBAs, including minimizing crystal defects, exploring transition metal ion doping, engineering electrode-electrolyte interfaces, and utilizing composite material designs are summarized. Despite the efforts devoted to the development and application of PBAs as PIB cathodes, research progress in this field is still in its infancy, and the electrochemical reaction mechanisms remain unclear. Therefore, several technical issues still need to be addressed in future laboratory research and industrialization of PBAs in PIBs, including the following aspects: Due to the hydrothermal synthesis conditions, crystalline water and interstitial water are inevitably introduced into the material matrix. A higher water content can trigger a series of water-related side reactions, leading to severe safety issues. The overall proportion of water molecules can be reduced by increasing the potassium content in the material. However, there is an upper limit of the potassium content in PBAs, and achieving an ideal state is restricted by the synthesis method. Relevant studies indicate that excessive dehydration can also compromise the structural stability of PBAs, highlighting the importance of selecting a reasonable proportion of water molecules in the synthesis process.
- (2) Owing to the strong electrostatic repulsion within the lattice, a large number of Fe(CN)<sub>6</sub> vacancies exist to maintain charge balance. These inert vacancies are embedded within the lattice and are unlikely to be fully activated, thus remaining stable during potassiation/depotassiation processes. Meanwhile, the interaction between Fe(CN)<sub>6</sub> vacancies and coordinated water molecules reduce the electrochemical activity of the PBA cathodes. Current chelating agent optimization strategies can effectively reduce the generation of vacancies; however, an increase in potassium content may still potentially adversely affect the stability and symmetry of the PBA crystal structure.
- (3) Currently, the optimization of PBAs structures has begun to exhibit redundancy. To further advance the commercialization of PIBs, further research should focus on electrolytes. Electrolytes significantly have a significant impact on the energy density and rate performance, especially in aqueous electrolyte systems. The different migration rates of potassium ions and electrons in the electrolyte result in charge imbalance on the surface of PBAs. This imbalance can lead to additional charge transfer at the interface, affecting potassium ion storage. Therefore, it is essential to further explore the interface between PBA cathodes and electrolytes to identify electrolytes that are more suitable for potassium ion transport. Additionally, the flammability of many organic electrolytes poses safety concerns that cannot be ignored. Consequently, research on electrolytes in PIBs should primarily aim at developing new formulations that combine three core characteristics: low concentration, high voltage resistance, and non-flammability. These three principles are crucial for advancing the development of next-generation safe and high-voltage PIBs.
- (4) Another important aspect that restricts the development of PIB is the choice of anode materials. Currently, anode materials for potassium-ion batteries include carbon-based materials (graphite, hard carbon, soft carbon, etc.), titanium-based materials, alloy materials, conversion materials and organic compounds. The prerequisite for commercializing potassium electricity is that the energy density and production cost of the battery can be matched, but each anode material has its own shortcomings. For example, conversion and alloy materials usually have high specific capacity, but the cost is high; titanium-based materials are cheap, but their low specific capacity cannot meet the practical application; organic polymers have poor thermal stability and pose safety hazards. Therefore, carbon-based materials are currently the most promising anode materials, but they also need to further solve the problem of low Coulomb efficiency for the first time.
- (5) To achieve large-scale applications of PIBs, the synthesis of PBAs should be optimized to be controllable, low-cost, and reproducible. Prior to entering the industrialization stage, researchers also need to identify the correlation between the synthesis process and the quality of the final products. There is still significant room for discussion and research on the crystal structure and reaction mechanisms of PBAs for the development of PBA cathodes. In the future, the potassium storage performance of PBAs can be further promoted through emerging strategies, such as the multi-

element substitution following the high-entropy strategy, in order to meet the demands of practical applications.

## 6. Declaration of Interests

The authors declare no competing interests.

## Acknowledgements

This work is supported by Research Start-up Funds of Nanjing Normal University (184080H201B41 and 184080H201B86)

## Conflict of Interests

The authors declare no conflict of interest.

**Keywords:** Prussian blue analogues · Potassium-ion batteries · Potassium storage mechanism · Cathode · Optimization strategies

- [1] F. M. N. U. Khan, M. G. Rasul, A. S. M. Sayem, N. K. Mandal, *J. Energy Storage*. **2023**, *71*, 108033.
- [2] K. Turcheniuk, D. Bondarev, G. G. Amatucci, G. Yushin, *Mater. Today*. **2021**, *42*, 57–72.
- [3] S. Chong, T. Li, S. Qiao, Y.-C. Yang, Z. Liu, J. Yang, H.-Y. Tuan, G. Cao, W. Huang, *ACS Nano*. **2024**, *18*, 3801–3813.
- [4] S. Chong, M. Ma, L. Yuan, S. Qiao, S. Dong, H. Liu, S. Dou, *Energy Environ. Mater.* **2023**, *6*, e12458.
- [5] M. Ma, S. Chong, K. Yao, H. K. Liu, S. X. Dou, W. Huang, *Matter*. **2023**, *6*, 3220–3273.
- [6] M. Ma, K. Yao, Y. Wang, D. Fattakhova-Rohlfing, S. Chong, *Adv. Funct. Mater.* **2024**, *34*, 2315662.
- [7] R. Verma, P. N. Didwal, J.-Y. Hwang, C.-J. Park, *Batteries & Supercaps*. **2021**, *4*, 1428–1450.
- [8] L. Wang, J. Zhu, N. Li, Z. Zhang, S. Zhang, Y. Chen, J. Zhang, Y. Yang, L. Tan, X. Niu, X. Wang, X. Ji, Y. Zhu, *Energy Environ. Sci.* **2024**, *17*, 3470–3481.
- [9] Y. Ouyang, P. Li, Y. Ma, J. Wei, W. Tian, J. Chen, J. Shi, Y. Zhu, J. Wu, H. Wang, *Small*. **2024**, *20*, 2308484.
- [10] H. Liang, Z. Sun, M. Zhang, W. Hu, J. Shi, J. Chen, W. Tian, M. Huang, J. Wu, H. Wang, *Energy Environ. Mater.* **2023**, *6*, e12559.
- [11] D. Qiu, Y. Hou, *Green Energy & Environ.* **2023**, *8*, 115–140.
- [12] L. Yang, Y. Zhao, Y. Zhang, C. Zhu, W. Wang, J. Shi, S. Liu, J. Chen, M. Huang, J. Wu, H. Wang, *Small Methods*. **2024**, *8*, 2301355.
- [13] H. Jeong, J. Jang, C. Jo, *Chem. Eng. J.* **2022**, *446*, 136860.
- [14] Q. Liu, H. Wang, C. Jiang, Y. Tang, *Energy Storage Mater.* **2019**, *23*, 566–586.
- [15] Y. Wu, H. Zhao, Z. Wu, L. Yue, J. Liang, Q. Liu, Y. Luo, S. Gao, S. Lu, G. Chen, X. Shi, B. Zhong, X. Guo, X. Sun, *Energy Storage Mater.* **2021**, *34*, 483–507.
- [16] Y.-S. Xu, S.-J. Guo, X.-S. Tao, Y.-G. Sun, J. Ma, C. Liu, A.-M. Cao, *Adv. Mater.* **2021**, *33*, 2100409.
- [17] S. M. Ahmed, G. Suo, W. A. Wang, K. Xi, S. B. Iqbal, *J. Energy Chem.* **2021**, *62*, 307–337.
- [18] Y. Yang, J. Zhou, L. Wang, Z. Jiao, M. Xiao, Q. Huang, M. Liu, Q. Shao, X. Sun, J. Zhang, *Nano Energy*. **2022**, *99*, 107424.
- [19] W.-J. Li, C. Han, G. Cheng, S.-L. Chou, H.-K. Liu, S.-X. Dou, *Small*. **2019**, *15*, 1900470.
- [20] W. Shu, C. Han, X. Wang, *Adv. Funct. Mater.* **2024**, *34*, 2309636.
- [21] X. Liu, Y. Cao, J. Sun, *Adv. Energy Mater.* **2022**, *12*, 2202532.
- [22] E. E. Levin, A. A. Kokin, D. E. Presnov, A. G. Borzenko, S. Y. V. Vassiliev, V. A. Nikitina, K. J. Stevenson, *ChemElectroChem*. **2020**, *7*, 761–769.
- [23] H. Li, W. Zhang, K. Sun, J. Guo, K. Yuan, J. Fu, T. Zhang, X. Zhang, H. Long, Z. Zhang, Y. Lai, H. Sun, *Adv. Energy Mater.* **2021**, *11*, 2100867.
- [24] A. Eftekhari, *J. Power Sources*. **2004**, *126*, 221–228.
- [25] G. He, L. F. Nazar, *ACS Energy Lett.* **2017**, *2*, 1122–1127.
- [26] W. Ren, X. Chen, C. Zhao, *Adv. Energy Mater.* **2018**, *8*, 1801413.
- [27] S. Chong, Y. Wu, S. Guo, Y. Liu, G. Cao, *Energy Storage Mater.* **2019**, *22*, 120.
- [28] M. Xia, X. Zhang, T. Liu, H. Yu, S. Chen, N. Peng, R. Zheng, J. Zhang, J. Shu, *Chem. Eng. J.* **2020**, *394*, 124923.
- [29] J. Ge, L. Fan, A. M. Rao, J. Zhou, B. Lu, *Nat. Sustain.* **2021**, *5*, 225–234.
- [30] Z. Wang, W. Zhuo, J. Li, L. Ma, S. Tan, G. Zhang, H. Yin, W. Qin, H. Wang, L. Pan, A. Qin, W. Mai, *Nano Energy*. **2022**, *98*, 107243.
- [31] R. Sun, X. Feng, J. Chen, Y. Zhang, R. Wang, Y. Chen, B. Han, K. Xia, Q. Gao, C. Zhou, *J. Power Sources*. **2023**, *556*, 232406.
- [32] X. Li, T. Guo, Y. Shang, T. Zheng, B. Jia, X. Niu, Y. Zhu, Z. Wang, *Adv. Mater.* **2024**, *36*, 2310428.
- [33] E. Goikolea, V. Palomares, S. Wang, I. R. de Larramendi, X. Guo, G. Wang, T. Rojo, *Adv. Energy Mater.* **2020**, *10*, 2002055.
- [34] X. Wu, Y. Ru, Y. Bai, G. Zhang, Y. Shi, H. Pang, *Coord. Chem. Rev.* **2022**, *451*, 214260.
- [35] S. Zhao, Z. Guo, K. Yan, X. Guo, S. Wan, F. He, B. Sun, G. Wang, *Small Structures*. **2021**, *2*, 2000054.
- [36] C. Peng, X. Xu, F. Li, L. Xi, J. Zeng, X. Song, X. Wan, J. Zhao, J. Liu, *Small Structures*. **2023**, *4*, 2300150.
- [37] W. Zhang, Y. Liu, Z. Guo, *Sci. Adv.* **2019**, *5*, eaav7412.
- [38] Y. Li, Q. Dang, W. Chen, L. Tang, M. Hu, *J. Inorg. Organomet. Polym.* **2021**, *31*, 1877–1893.
- [39] Y. Wang, F. Zhang, Q. Long, S. Li, D. Guo, Z. Zhu, H. Zhang, *Energy Storage Mater.* **2024**, *71*, 103399.
- [40] S. Wheeler, I. Capone, S. Day, C. Tang, M. Pasta, *Chem. Mater.* **2019**, *31*, 2619–2626.
- [41] A. J. Mayer, O. T. Beynon, A. J. Logsdail, K. G. Upul Wijayantha, S. E. Dann, J. F. Marco, J. D. Elliott, M. Aramini, G. Cibin, S. A. Kondrat, *J. Mater. Chem. A*. **2023**, *11*, 19900–19913.
- [42] Z. Shadike, D.-R. Shi, Tian-Wang, M.-H. Cao, S.-F. Yang, J. Chen, Z.-W. Fu, *J. Mater. Chem. A*. **2017**, *5*, 6393–6398.
- [43] Y. Bai, K. YuChi, X. Liu, S. Tian, S. Yang, X. Qian, B. Ma, M. Fang, Y. Liu, Z. Huang, X. Min, *Eur. J. Inorg. Chem.* **2023**, *26*, e202300246.
- [44] H. L. B. Boström, I. E. Collings, D. Daisenberger, C. J. Ridley, N. P. Funnell, A. B. Cairns, *J. Am. Chem. Soc.* **2021**, *143*, 3544–3554.
- [45] B. Han, D. Zhang, X. Liu, Z. Wang, W. Qu, S. Zhang, C. Deng, *J. Mater. Chem. A*. **2022**, *10*, 13508–13518.
- [46] Y. Yang, E. Liu, X. Yan, C. Ma, W. Wen, X.-Z. Liao, Z.-F. Ma, *J. Electrochem. Soc.* **2016**, *163*, A2117.
- [47] Y. Huang, M. Xie, Z. Wang, Y. Jiang, Y. Yao, S. Li, Z. Li, L. Li, F. Wu, R. Chen, *Small*. **2018**, *14*, 1801246.
- [48] B. Xie, P. Zuo, L. Wang, J. Wang, H. Huo, M. He, J. Shu, H. Li, S. Lou, G. Yin, *Nano Energy*. **2019**, *61*, 201–210.
- [49] A. Zhou, W. Cheng, W. Wang, Q. Zhao, J. Xie, W. Zhang, H. Gao, L. Xue, J. Li, *Adv. Energy Mater.* **2021**, *11*, 2000943.
- [50] X. Wu, M. Sun, S. Guo, J. Qian, Y. Liu, Y. Cao, X. Ai, H. Yang, *ChemNanoMat*. **2015**, *1*, 188–193.
- [51] T. Masese, G. M. Kanyolo, *Energy Adv.* **2024**, *3*, 60–107.
- [52] J. Peng, W. Zhang, Q. Liu, J. Wang, S. Chou, H. Liu, S. Dou, *Adv. Mater.* **2022**, *34*, 2108384.
- [53] B. Singh, A. Indra, *Mater. Today Energy*. **2020**, *16*, 100404.
- [54] H. Yi, R. Qin, S. Ding, Y. Wang, S. Li, Q. Zhao, F. Pan, *Adv. Funct. Mater.* **2021**, *31*, 2006970.
- [55] C. Li, T. Ni, M. Yue, S. Li, Q. Zhang, *Batteries & Supercaps*. **2024**, e202400138.
- [56] J. Liu, Z. Shen, C.-Z. Lu, *J. Mater. Chem. A*. **2024**, *12*, 2647–2672.
- [57] W. Wang, Z. Hu, Z. Yan, J. Peng, M. Chen, W. Lai, Q.-F. Gu, S.-L. Chou, H.-K. Liu, S.-X. Dou, *Energy Storage Mater.* **2020**, *30*, 42–51.
- [58] L. Li, Z. Hu, Y. Lu, C. Wang, Q. Zhang, S. Zhao, J. Peng, K. Zhang, S.-L. Chou, J. Chen, *Angew. Chem. Int. Ed.* **2021**, *133*, 13160–13166.
- [59] W. Shu, M. Huang, L. Geng, F. Qiao, X. Wang, *Small*. **2023**, *19*, 2207080.
- [60] V. Renman, D. O. Ojwang, C. Pay Gómez, T. Gustafsson, K. Edström, G. Svensson, M. Valvo, *J. Phys. Chem. C*. **2019**, *123*, 22040–22049.
- [61] B. Huang, Y. Shao, Y. Liu, Z. Lu, X. Lu, S. Liao, *ACS Appl. Energ. Mater.* **2019**, *2*, 6528–6535.
- [62] J. Lin, R. Chenna Krishna Reddy, C. Zeng, X. Lin, A. Zeb, C.-Y. Su, *Coord. Chem. Rev.* **2021**, *446*, 214118.
- [63] J. Cattermull, M. Pasta, A. L. Goodwin, *Mater. Horiz.* **2021**, *8*, 3178–3186.
- [64] H. Li, J. Huang, K. Yang, Z. Lu, S. Yan, H. Su, C. Liu, X. Wang, B. Ren, *J. Phys. Chem. Lett.* **2022**, *13*, 479–485.
- [65] C. Li, X. Wang, W. Deng, C. Liu, J. Chen, R. Li, M. Xue, *ChemElectroChem*. **2018**, *5*, 3887–3892.

- [66] S. Jung, P. T. Huong, M. Mapari, T. Thanh Tung, T. Kim, *Batteries & Supercaps* **2024**, *7*, e202400091.
- [67] R. Ma, Z. Wang, Q. Fu, W. Zhou, Y. Mo, J. Tu, Z. Wang, P. Gao, C. Fan, J. Liu, *J. Energy Chem.* **2023**, *83*, 16–23.
- [68] L. Ni, G. Xu, C. Li, G. Cui, *Exploration* **2022**, *3*, 20210239.
- [69] S. Liu, L. Kang, S. C. Jun, *Adv. Mater.* **2021**, *33*, 2004689.
- [70] J. Qian, C. Wu, Y. Cao, Z. Ma, Y. Huang, X. Ai, H. Yang, *Adv. Energy Mater.* **2018**, *8*, 1702619.
- [71] L. Deng, J. Qu, X. Niu, J. Liu, J. Zhang, Y. Hong, M. Feng, J. Wang, M. Hu, L. Zeng, Q. Zhang, L. Guo, Y. Zhu, *Nat. Commun.* **2021**, *12*, 2167.
- [72] Y. Lin, J. Liu, L. Shi, N. Guo, Z. Sun, C. Geng, J. Jiang, Q. Zhuang, Y. Chen, Z. Ju, *J. Colloid Interface Sci.* **2022**, *623*, 1–8.
- [73] A. Li, Y. Man, J. Liao, L. Duan, X. Ji, X. Zhou, *Nano Lett.* **2023**, *23*, 10066–10073.
- [74] C. Gao, Y. Lei, Y. Wei, H. Wang, F. Yuan, F. Kang, D. Zhai, *Chem. Eng. J.* **2022**, *431*, 133926.
- [75] X. Chen, Y. Xia, X. Fang, K. Zhang, Y. Xiong, Z. Jian, *J. Mater. Sci.* **2022**, *57*, 14015–14025.
- [76] U. Ali, B. Liu, H. Jia, Y. Li, Y. Li, Y. Hao, L. Zhang, S. Xing, L. Li, C. Wang, *Small* **2024**, *57*, 2305866.
- [77] B. Huang, Y. Liu, Z. Lu, M. Shen, J. Zhou, J. Ren, X. Li, S. Liao, *ACS Sustainable Chem. Eng.* **2019**, *7*, 16659–16667.
- [78] Q. Zhou, H. K. Liu, S. X. Dou, S. Chong, *ACS Nano* **2024**, *18*, 7287–7297.
- [79] Y. Ma, Y. Ma, S. L. Dreyer, Q. Wang, K. Wang, D. Goonetilleke, A. Omar, D. Mikhailova, H. Hahn, B. Breitung, T. Brezesinski, *Adv. Mater.* **2021**, *33*, 2101342.
- [80] Y. He, S. L. Dreyer, Y. Ting, Y. Ma, Y. Hu, D. Goonetilleke, Y. Tang, T. Diemant, B. Zhou, P. M. Kowalski, M. Fichtner, H. Hahn, J. Aghassi-Hagmann, T. Brezesinski, B. Breitung, Y. Ma, *Angew. Chem. Int. Ed.* **2023**, *136*, e202315371.
- [81] Y. Ma, T. Brezesinski, B. Breitung, Y. Ma, *Matter* **2023**, *6*, 313–315.
- [82] Y. Ma, Y. Hu, Y. Pramudya, T. Diemant, Q. Wang, D. Goonetilleke, Y. Tang, B. Zhou, H. Hahn, W. Wenzel, M. Fichtner, Y. Ma, B. Breitung, T. Brezesinski, *Adv. Funct. Mater.* **2022**, *32*, 2202372.
- [83] B. Liu, Q. Zhang, L. Zhang, X. Yong, L. Li, C. Wang, *Energy Storage Mater.* **2024**, *66*, 103221.
- [84] C. Ma, C. Lin, N. Li, Y. Chen, Y. Yang, L. Tan, Z. Wang, Q. Zhang, Y. Zhu, *Small* **2024**, *20*, 2310184.
- [85] X. Ma, J. Chen, C. Yu, J. Sun, X. Cao, Z. Cheng, Y. Guo, X. Wang, Z. Zi, J. Dai, *J. Electroanal. Chem.* **2022**, *918*, 116468.
- [86] J. Dong, Y. Lei, D. Han, H. Wang, D. Zhai, B. Li, F. Kang, *Chem. Commun.* **2019**, *55*, 12555–12558.
- [87] Q. Xue, L. Li, Y. Huang, R. Huang, F. Wu, R. Chen, *ACS Appl. Mater. Interfaces* **2019**, *11*, 22339–22345.
- [88] Y. Zhu, Y. Yin, X. Yang, T. Sun, S. Wang, Y. Jiang, J. Yan, X. Zhang, *Angew. Chem. Int. Ed.* **2017**, *56*, 7881–7885.
- [89] F. Chen, J. Liao, J. Wang, X. He, X. Ding, Q. Hu, F. Chen, S. Wang, J. Dong, Z. Wen, C. Chen, *Chem. Commun.* **2020**, *56*, 9719–9722.
- [90] L. Fan, H. Xie, Y. Hu, Z. Caixiang, A. M. Rao, J. Zhou, B. Lu, *Energy Environ. Sci.* **2023**, *16*, 305–315.
- [91] Y. Geng, H. Fu, Y. Hu, A. M. Rao, L. Fan, J. Zhou, B. Lu, *Appl. Phys. Lett.* **2024**, *124*, 063901.
- [92] Y. Hu, H. Fu, Y. Geng, X. Yang, L. Fan, J. Zhou, B. Lu, *Angew. Chem. Int. Ed.* **2024**, *136*, e202403269.
- [93] X. Ma, H. Fu, J. Shen, D. Zhang, J. Zhou, C. Tong, A. M. Rao, J. Zhou, L. Fan, B. Lu, *Angew. Chem. Int. Ed.* **2023**, *62*, e202312973.
- [94] S. Liu, J. Mao, Q. Zhang, Z. Wang, W. K. Pang, L. Zhang, A. Du, V. Sencadas, W. Zhang, Z. Guo, *Angew. Chem. Int. Ed.* **2020**, *59*, 3638–3644.
- [95] H. Zhang, H. Wang, W. Li, Y. Wei, B. Wen, D. Zhai, F. Kang, *Adv. Funct. Mater.* **2024**, *34*, 2312368.
- [96] X. Jiang, T. Zhang, L. Yang, G. Li, J. Y. Lee, *ChemElectroChem* **2017**, *4*, 2237–2242.
- [97] K. Luo, Z. Wang, Y. Mo, J. Ke, W. Zhou, K. Wang, S. Chen, P. Gao, A. Hu, J. Liu, *Adv. Funct. Mater.* **2024**, *34*, 2311364.
- [98] H. Zhang, C. Luo, H. He, H.-H. Wu, L. Zhang, Q. Zhang, H. Wang, M.-S. Wang, *Nanoscale Horiz.* **2020**, *5*, 895–903.
- [99] Y. Wei, H. Wang, J. Wang, C. Gao, H. Zhang, F. Yuan, J. Dong, D. Zhai, F. Kang, *ACS Appl. Mater. Interfaces* **2021**, *13*, 54079–54087.
- [100] J. Zhang, L. Deng, M. Feng, L. Zeng, M. Hu, Y. Zhu, *Chem. Commun.* **2021**, *57*, 8632–8635.
- [101] E. Nossol, V. H. R. Souza, A. J. G. Zarbin, *J. Colloid Interface Sci.* **2016**, *478*, 107–116.
- [102] S. Husmann, A. J. G. Zarbin, R. A. W. Dryfe, *Electrochim. Acta* **2020**, *349*, 136243.
- [103] M. Morant-Giner, R. Sanchis-Gual, J. Romero, A. Alberola, L. García-Cruz, S. Agouram, M. Galbiati, N. M. Padial, J. C. Waerenborgh, C. Martí-Gastaldo, S. Tatay, A. Forment-Aliaga, E. Coronado, *Adv. Funct. Mater.* **2018**, *28*, 1706125.
- [104] X. Li, X. Zhang, J. Xu, Z. Duan, Y. Xu, X. Zhang, L. Zhang, Y. Wang, P. K. Chu, *Adv. Sci.* **2024**, *11*, 2305467.

Manuscript received: July 1, 2024

Revised manuscript received: August 29, 2024

Accepted manuscript online: September 2, 2024

Version of record online: October 24, 2024